Real-time detection of methane emission for monitoring intestinal microcirculatory changes

Ph.D. Thesis

Anett Gabriella Bársony M.D.

University of Szeged

Albert Szent-Györgyi Medical School

Doctoral School of Multidisciplinary Medical Sciences

Institute of Surgical Research

Supervisors: Gabriella Varga Ph.D.

Dániel Érces M.D., Ph.D.

Szeged

2025

LIST OF PUBLICATIONS

Full papers related to the subject of the thesis

I. **Bársony A**, Vida N, Gajda Á, Rutai A, Mohácsi Á, Szabó A, Boros M, Varga G, Érces D. Methane Exhalation Can Monitor the Microcirculatory Changes of the Intestinal Mucosa in a Large Animal Model of Hemorrhage and Fluid Resuscitation. *Front Med* 2020; 7:567260. doi: 10.3389/fmed.2020.567260. eCollection 2020. **IF: 4.59**

II. Ugocsai M, **Bársony A,** Varga RA, Gajda Á, Vida N, Lajkó N, Rónaszéki B, Tóth G, Boros M, Érces D, Varga G. Conjugation with Tris decreases the risk of ketoprofen-induced mucosal damage and reduces inflammation-associated methane production in a rat model of colitis. *Pharmaceutics* 2023; 15 (9): 2329 **IF: 3.24**.

∑ Impact factor: 7.83

Full paper closely related to the subject but not included in the thesis

I. Vida N, Varga Z, Szabó-Biczók A, Bari G, Vigyikán G, Hodoniczki Á, Gajda Á, RutaiA, Juhász L, Tallósy SP, Turkevi-Nagy S, **Bársony A**, Öveges N, Szabó A, Boros M, Varga, G, Érces D. Methane administration during oxygenation mitigates acute kidney injury in a pig model of 24-hour veno-venous extracorporeal membrane oxygenation. *Shock* 2025; *in press* **IF: 2.7**

Full paper not related to the subject of the thesis

I. Lázár G, Paszt A, Simonka Z, **Bársony A**, Ábrahám S, Horváth G. A successful strategy for surgical treatment of Boerhaave's syndrome. *Surgical endoscopy*. 2011; 25(11), 3613-3619. DOI: 10.1007/s00464-011-1767-1 **IF: 4.013**

∑ Impact factor: 15.25

LIST OF ABBREVIATIONS

BV – blood volume

DBS – De Backer's score

GC – gas chromatography

GI – gastrointestinal

Hct – haematocrit

HES – hydroxyethyl starch

HI – heterogeneity index

IBD – inflammatory bowel disease

IVM – intravital microscopy

Ket – ketoprofen

MAP – mean arterial pressure

MDA – malondialdehyde

MFI – microvascular flow index

MPO – myeloperoxidase

NSAID – non-steroidal anti-inflammatory drug

OPS – orthogonal polarization spectral imaging

PAS – photoacoustic spectroscopy

RBCV – red blood cell velocity

ROS – reactive oxygen species

SMA – superior mesenteric artery

tHb – total haemoglobin

TNBS – 2,4,6-trinitrobenzenesulfonic acid

Tris – 2-amino-2-(hydroxymethyl)-1,3-propanediol

XOR – xanthine oxidoreductase

SUMMARY

Acute gastrointestinal (GI) circulation changes are common in critical conditions and can lead to significant morbidity and mortality, highlighting the need for monitoring microcirculatory changes for better intervention strategies. Current assessment methods, such as indirect tonometry and sublingual microcirculation analysis, show limited reliability, necessitating alternative approaches. Measurement of exhaled methane offers diagnostic potential and can aid in the early detection of GI circulatory disturbances, being utilized currently for conditions like malabsorption syndromes. Traditional gas chromatography (GC) techniques, however, are artifact-prone; thus, we propose using photoacoustic spectroscopy (PAS) for real-time, sensitive methane monitoring to assess GI macro- and microcirculation changes.

We conducted two studies investigating methane emission measurement's diagnostic potential. Study 1 focused on the relationship between methane emissions and GI microcirculation disturbances in rat models of trinitrobenzene-sulfonic acid (TNBS) colitis and drug-induced alterations. Study 2 validated real-time breath methane detection in a large animal model undergoing controlled haemorrhage and resuscitation, comparing it to sublingual microcirculatory examination.

Whole-body methane emissions were significantly elevated during experimental colitis, linked to hyperemia and oxidative stress, suggesting its potential as a biomarker for GI inflammation. Ketoprofen (Ket) administration enhanced methane emissions compared to Ket-2-amino-2-(hydroxymethyl)-1,3-propanediol (Ket-Tris) conjugate, indicating distinct microcirculatory effects of these compounds. Real-time monitoring of methane levels enabled insights into microcirculatory responses to drugs, proposing utility in tracking inflammatory processes in the GI tract.

Continuous methane detection during haemorrhage showed relationships between methane levels and mesenteric blood flow, demonstrating methane's potential as a real-time marker of altered GI circulation. Changes in exhaled methane concentrations reflected alterations in ileal microcirculation earlier than changes in sublingual circulation during resuscitation phases.

Based on our results methane emission may serve as early indicator of GI inflammation or bleeding, reflecting mesenteric perfusion changes during GI inflammatory processes and subsequent treatments. This method's diagnostic value is comparable to monitoring sublingual microcirculation. Thus, methane emission measurement can be valuable as a non-invasive tool in clinical scenarios involving anticipated haemorrhagic complications or inaccessible GI tract areas and enhancing insights into mesenteric circulation within experimental contexts.

1. INTRODUCTION

1.1 Blood supply and perfusion system of the intestinal tract

The vascular architecture of the intestinal tract is characterized by a complex network of arterioles that ultimately contribute to the perfusion of the intestinal wall. These arterioles extend into the vasa recta, a network of blood vessels within the mesentery that envelops the entire musculature of the intestinal tract. Upon reaching the submucosal layer, these arterioles converge to form an arterial plexus, which serves as a critical conduit for blood flow. From this plexus, the arterioles penetrate the mucous membrane, subsequently branching into longitudinal muscle layers where they give rise to parallel capillary networks. Quantitatively, it has been observed that approximately 20% of the blood circulating within the intestinal wall traverses the muscle layers, while a significant 80% is directed through the mucous membrane. The contractile activity of the intestinal musculature is primarily localized to the muscle layers, whereas the tension exerted on the intestinal wall plays a pivotal role in modulating the flow dynamics within the capillary networks of the mucous membrane. The capillary network within the mucous membrane exhibits distinct variations across different segments of the intestinal tract, reflecting the specialized microcirculatory architecture inherent to each region. In humans, the arterioles supplying the mucosa of the small intestine are intricately adapted to the structural characteristics of the intestinal villi. Each villus is associated with a rich capillary network at its apex, supplied by a non-centrally located arteriole and venule, facilitating efficient nutrient absorption and exchange. Conversely, in the colon, the arterioles are oriented parallel to the mucosal glands, and the surface capillary network formed in this region is situated closer to the epithelial layer than in the small intestine. When viewed from the lumen, the capillaries within the mucous membrane exhibit a honeycomb-like morphology, characterized by a specific geometric arrangement. Notably, the density of this capillary network diminishes along the proximo-distal axis of the large intestine, indicating a gradient in perfusion and possibly reflecting the differing functional demands of the intestinal segments (Kvietys, 2010)

1.2 Inflammatory diseases in the intestinal tract

Inflammatory bowel disease (IBD) is a complex, idiopathic condition characterized by chronic, immune-mediated inflammation of the gastrointestinal (GI) tract. Clinically and histologically, IBD is primarily categorized into two distinct forms: Crohn's disease and ulcerative colitis. The significance of IBD is increasingly recognized, as evidenced by a notable

rise in incidence rates, even in regions previously considered unaffected. This trend is particularly pronounced in Western countries, where advanced disease management strategies have led to a higher prevalence of the condition (Ng et al, 2017). The evolving pathological landscape of IBD has profound implications for treatment strategies. A comprehensive understanding of the underlying pathophysiology of IBD facilitates the identification of multiple intervention points and target molecules, thereby laying the groundwork for the development of novel pharmaceutical agents that can significantly enhance disease prognosis. Consequently, it is essential not only to be well-versed in current therapeutic modalities but also to remain informed about potential future pharmacological innovations.

The primary objectives of IBD treatment encompass the reduction of inflammation, the prevention of complications, and the enhancement of the patient's quality of life. Treatment approaches can be broadly classified into pharmacological and surgical interventions aimed at managing complications. Within the realm of pharmacotherapy, two main categories of medicinal products are utilized in clinical practice. The first category includes "traditional" pharmaceutical agents, such as 5-aminosalicylates, corticosteroids, cytotoxic agents, and antibiotics, as well as probiotics. The second category encompasses biological therapies, which include anti-TNFα agents (Rutgeerts et al, 2004), anti-integrin agents, and monoclonal antibodies targeting interleukin-12/23 (Steigleder et al, 2020). A significant proportion of patients exhibit resistance to anti-TNFα antibodies, underscoring the urgent need for the development of alternative therapeutic agents. Promising candidates for future pharmacological interventions include homing inhibitors, Janus kinase inhibitors, Th17 inhibitors, and sphingosine-1-phosphate receptor agonists. The societal impact of IBD is further accentuated by its prevalence among young adults, thereby imposing a considerable burden on healthcare systems. With appropriate therapeutic strategies, patients with IBD can achieve a favorable prognosis and a marked improvement in quality of life - an especially important outcome given the high prevalence of the disease among younger individuals. Ongoing advancements in medical science, particularly the introduction of novel pharmacological agents, offer an increasingly optimistic outlook for those affected by IBD (Rutgeerts et al, 2004; Steigleder et al, 2020).

To further improve treatment outcomes, the development of innovative diagnostic tools is essential. Continuous, real-time monitoring of microperfusion in the lower GI tract could significantly deepen our understanding of the microcirculatory disturbances linked to IBD. Such monitoring would not only help assess treatment efficacy but also enable the early

detection of disease flares, thereby allowing timely initiation of therapy. In this context, we propose the measurement of methane emissions as a promising, non-invasive method to support these diagnostic aims.

1.3 Acute changes in the intestinal macro- and microcirculation: Why and how to monitor?

Acute changes in the GI circulation and microcirculation are significant, multi-faceted medical problems. They are common, but often overlooked consequences of acute clinical disorders, including haemorrhage, inflammatory processes, embolism, thrombosis, trauma, external compression or low cardiac output. Moreover, impaired GI perfusion, and subsequent reperfusion is a decisive factor in the mortality and morbidity in many cases of vascular, reconstructive-, or transplant surgery.

The manifestation of internal haemorrhage, which can be a frequent complication in the aforementioned situations, is heterogeneous, with clinical signs and symptoms often being subtle and challenging to discern; consequently, reaching an accurate diagnosis may prove difficult (Kassavin et al, 2011). During the initial phase of haemorrhage, hemodynamic changes or deviations in routine laboratory parameters frequently remain absent. Furthermore, advanced imaging modalities, such as multidetector computed tomography and catheter angiography (Kim et al, 2014; Tasu et al, 2015; Kumar et al, 2017) which possess the capacity to detect the presence and localization of haemorrhagic events, are often either inaccessible or unsuitable for continuous monitoring.

Moreover, according to the relevant literature, the macro- and microhemodynamics may change relatively independently or may be dissociated in stress conditions, i.e. the macrohemodynamics is usually not able to predict the ensuing microcirculatory changes correctly and timely. A peripheral microcirculatory dysfunction frequently develops in critically ill patients, even if the goals of macrohemodynamic resuscitation are achieved (Dubin et al, 2009; Jhanji et al, 2009). These microhemodynamic alterations can contribute to the development of organ failure and may be of prognostic importance, too (De Backer et al, 2010).

The possibility to monitor the changes of GI microperfusion is of fundamental importance for the success of treatment. Early diagnosis of altered GI perfusion is mandatory to start the necessary interventions as soon as possible - to prevent the development of mucosal damage, and the loss of the barrier function. Nevertheless, the tracking of the microcirculatory changes is not easy; the access to the intraabdominal areas is difficult, even during experimental

conditions. Indirect tonometry is applied with various success rates, but at present the only available and clinically useful non-invasive technique is the analysis of the sublingual circulation with intravital microscopy (IVM). This allows the estimation of the condition of the oral section of GI tract indirectly, but the relevant international literature is ambiguous, and there are many contradictory data on the reliability of the method (Boerma et al, 2007; Qian et al, 2014).

1.4 Endogenous methane production: diagnostic importance

Based on this background we proposed a solution to this problem, the real-time, continuous measurement of exhaled methane concentrations. Endogenous methane production in humans has garnered attention for its potential physiological significance, particularly in relation to cellular processes and membrane dynamics. According to Boros et al. (2012), it is hypothesized that methane may accumulate at cell membrane interfaces, thereby influencing the physicochemical properties and functionality of membrane-bound proteins, including enzymes involved in reactive oxygen species (ROS) production. This accumulation could modulate the activity of membrane channels and enzymes, potentially altering cellular signaling pathways and redox balance (Boros and Keppler, 2019). Furthermore, recent studies have confirmed that all humans produce and exhale methane, suggesting that this process may be an inherent aspect of human physiology (Keppler et al, 2016). While the exact role of endogenous methane in human health remains to be fully elucidated, it is posited that it could serve as a gasotransmitter, impacting various biological functions and possibly providing protective effects against oxidative stress (Boros and Keppler, 2019). Understanding the mechanisms of endogenous methane production and its implications for cellular function may open new avenues for therapeutic interventions in conditions associated with oxidative stress and inflammation.

Nevertheless, the methane production in humans can also be primarily attributed to specific methanogenic archaea found in the GI tract, with Methanobrevibacter smithii being the predominant species. These microorganisms utilize hydrogen produced during the fermentation of undigested carbohydrates to synthesize methane as a metabolic by-product.

Due to its physicochemical properties, methane is distributed evenly across membrane barriers, traverses the mucosa and enters the splanchnic microcirculation freely. It follows that a larger portion of the produced amount is transported to the alveoli by the circulation and then exhaled through the lungs. Breath tests therefore have become a tool for the diagnosis of certain

GI conditions. Nevertheless, it is important to note that only 30-40% of the population in Western societies is considered methane producer (Levitt et al, 2006), according to the methane levels measured in the exhaled air. Today it is believed that methane producers and non-producers are distinct human populations distinguished by methane breath testing using lactulose ingestion. Being a methane producer is usually defined as more than 1 ppm methane level in the exhaled air over the atmospheric concentration (Bond et al, 1971). Nevertheless, it is equally possible that the non-producer status also related with endogenous methane generation, which occurs at a rate and dynamics which is impossible to detect with the currently used methods. It is noteworthy that the proportion of methane producers has remained relatively stable during recent decades, despite changes in GI medication and diets (Levitt et al, 2006).
Exhaled methane measurement has been applied for testing various medical conditions related with malabsorption syndromes. In such cases, the output of methane or methyl group-containing compounds is usually measured in exhaled air samples by means of GC or GC-mass spectrometry (Levitt et al, 2006; Ligor et al, 2008). These traditional methods of gas analysis have many limitations, and the risk of possible artefacts is very high (Yu and Pawliszyn, 2004). Furthermore, discontinuous detection methods cannot reflect the overall profile of in vivo methane release. Detection of methane content of the exhaled air has not been considered as a monitoring possibility for the condition of the intestinal microcirculation, yet. However, this idea was supported by an observation in a porcine sepsis model. In animals with severe hyperdynamia, which evolved in the early stages of sepsis, higher levels of exhaled methane were demonstrated (Kaszaki et al, 2013).

For continuous methane detection, and as a technical basis for a monitoring approach, near-infrared diode lasers are very effective tools. High-sensitivity photoacoustic spectroscopy (PAS)-based methane sensors have been reported in the literature (Ngai et al, 2006). During PAS measurements, sound waves are generated because of light absorption by a sample. The absorption of light causes the molecules of gases and vapors to transition from their ground state to an excited state. The subsequent relaxation from this excited state induces localized heating in the vicinity of the excitation source, leading to the formation of a periodic pressure variation, which manifests as sound. This sound can be detected using appropriate acoustic detection devices (Bozóki et al, 2011). A tunable laser serves as the excitation source, therefore enhanced specificity of the photoacoustic effect can be achieved, as it is only observed at the wavelengths where the sample exhibits significant absorption (Michelian, 2010).

Our purpose-built PAS instrument allows for in situ, continuous measurements for methane with very high sensitivity. We have already provided evidence that this breath analysis device can successfully substitute GC (Tuboly et al, 2013).

2 MAIN GOALS

In our earlier proof-of-concept study, we provided evidence that exhaled methane levels fluctuate in association with changes in superior mesenteric arterial blood flow (Szűcs et al, 2019). It was demonstrated that arterial occlusions and reperfusions, as well as the accompanying cycles of mucosal microcirculatory disturbances, significantly correlated with parallel changes in exhaled methane concentrations. Therefore, the primary aim of the first study in this thesis was to investigate the diagnostic potential of whole-body methane emissions in rat models under the following conditions: (1) chemically induced GI microcirculatory disturbances and inflammatory responses (2,4,6-trinitrobenzenesulfonic acid (TNBS) colitis), (2) drug-induced GI microcirculatory alterations, and (3) a combined application of both (1) and (2). Additionally, in model (1), we examined the relationship between the inflammatory response and altered methane production.

In doing so, we built upon previous findings suggesting that methane may be released under pro-inflammatory conditions or during transient tissue hypoxia (Ghyczy et al, 2008). While biogenic methane in the mammalian GI tract is traditionally produced by methanogenic archaea under strict anaerobic conditions (Conrad, 2009; Ellermann et al, 1988), recent studies on plant, animal, and human cells have revealed that methane can also be generated under specific redox conditions associated with ROS formation - even in the presence of oxygen and in the absence of specific enzymes (Boros and Keppler, 2019). Once produced, GI methane is transported via the splanchnic microcirculation to the lungs and partially exhaled - provided that its partial pressure exceeds that of the ambient air. Additional quantities may be discharged through the skin and natural orifices (Boros et al, 2015). Given that local ROS generation is an early homeostatic response to GI microcirculatory distress and inflammation, we hypothesized that methane emission monitoring could serve as a potential indicator of ROS-driven mucosal activity. To explore this, we also assessed enzymatic activity and oxidative stress markers in relation to methane output.

In the second study, our goal was to evaluate the diagnostic value of real-time exhaled methane measurement in detecting internal bleeding, using a clinically relevant large-animal model. We investigated whether continuous monitoring of exhaled methane could reflect the condition of

the mesenteric vascular bed during hemorrhage and fluid resuscitation. Furthermore, we compared the diagnostic performance of this method with that of sublingual microcirculation assessment using intravital videomicroscopy - specifically, incident dark field and orthogonal polarization spectral (OPS) imaging, both of which are clinically employed but indirect techniques.

Summary of objectives

The overarching aim of this research was to thoroughly investigate the relationship between methane emission and GI microcirculation. More specifically, the primary objective of the first study was to explore the association between whole-body methane emission, colonic mucosal inflammation, and the microcirculation of the colonic and small intestinal serosa in experimental rat models.

1. Our goal was to demonstrate the connection between whole-body methane emission and the microcirculatory and inflammatory changes in the colon and small intestine induced by TNBS-triggered experimental colitis.
2. Furthermore, we examined how drug-induced alterations in GI microcirculation affect methane emission levels.
3. An additional aim was to assess how whole-body methane production changes in response to colonic mucosal microcirculatory disturbances during TNBS-induced colitis, and how these responses are modulated by Ketoprofen (Ket) and Ket-Tris (Ket-Tris) treatments.

In the second part of the research, our objective was to validate and compare the sensitivity of real-time exhaled methane monitoring against an established method - sublingual microcirculatory assessment - within a large animal model of controlled, graded hemorrhage followed by the early phase of fluid resuscitation.

4. We aimed to evaluate the diagnostic potential of real-time exhaled methane detection for identifying internal bleeding in a large animal model, correlating changes in methane output with superior mesenteric arterial blood flow and mucosal microcirculatory parameters.
5. Additionally, we sought to determine whether continuous breath methane monitoring could offer clinically relevant insights into the state of the mesenteric vascular bed during the early stages of fluid resuscitation.

3 MATERIALS AND METHODS

3.1 Study 1: Diagnostic significance of whole-body methane emission in detection of GI microcirculatory alterations and inflammation

3.1.1 Animals and chemicals

The experiments were performed in three separate but interlinked studies (Fig. 2, 3, 4) on male Sprague-Dawley rats (n=72; average weight 200 g ± 10 g) housed in plastic cages under a 12-h dark-light cycle, in a thermoneutral environment (21±2 °C). The animals were kept on normal laboratory chow and then for 3 days prior to the experiments all of them were fed with a carbohydrate-rich diet (bread rolls). In case of anaesthesia, the animals were deprived of food, but not water for 12 h prior to the experiments. The protocols were in accordance with EU directive 2010/63 for the protection of animals used for scientific purposes and were approved by the National Scientific Ethical Committee on Animal Experimentation (National Competent Authority) with the licence number V./148/2013. This study also complied with the criteria of the US National Institutes of Health Guidelines for the Care and Use of Laboratory Animals.

During the investigations, we utilized TNBS (Sigma-Aldrich GmbH, Steinheim, Germany) to induce colitis. To mitigate the resulting inflammation, the animals were treated with either Ket (Sigma-Aldrich GmbH, Steinheim, Germany) or a Ket-Tris conjugate (were synthetized in the Department of Medical Chemistry, University of Szeged; *Miklós Ghyczy was until 09.2016 applicant and proprietor of European patent application EP 2889286A1 and International patent application WO 2015/101501 (PCT/EP2014/078296) entitled "Pharmaceutically active compound for use as anti-inflammatory agent"*).

3.1.2 Experimental protocol of Study 1/1: Connection among whole-body methane emission microcirculatory change and inflammatory response induced by experimental TNBS-colitis.

In Study 1/1 the animals (n=30) were randomly allocated into 2 groups (n=15, each). In group 1 colitis was induced by the intracolonic (ic) administration of TNBS (40 mg/kg in 0.25 ml of 25% ethanol) through an 8 cm-long soft plastic catheter under transient light inhalation anaesthesia (Morris et al, 1989). In control group, the animals received enemas with a total volume of 0.25 ml containing 25% of ethanol (the solvent for TNBS). The animals were then returned to their cages and were fed *ad libitum* with standard laboratory chow. On days 1, 2 and

3 after colitis induction 5-5 animals of each group were anesthetized for invasive microcirculatory investigations and biochemical sample collection. Besides, whole body methane detection was performed individually in the same timeframes (see later). (Figure 1)

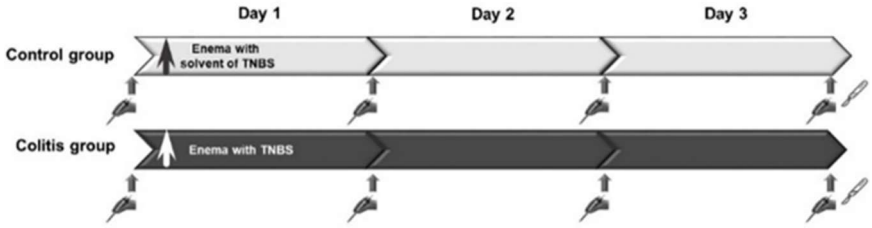

Figure 1. *Experimental protocol and timeline of Study 1/1*

3.1.3 Experimental protocol Study 1/2: Connection between whole-body methane emission and drug induced GI microcirculatory changes.

In Study 1/2, the animals (n=18) were randomly allocated into 3 groups (n=6, each). Group 1 served as vehicle-treated control where 10 ml/kg buffered 0.11 M potassium hydroxide (KOH) was given orally. In group 2, high doses of Ket solution (0.56 mmol/kg, in a volume of 10 ml/kg) were gavaged via a flexible oesophageal tube to the animals. After the treatment, the animals were returned to their cages and were fed *ad libitum* with a carbohydrate-rich diet. Group 3 was treated with the Ket-Tris conjugate in equimolar doses to Ket (0.56 mmol/kg, in a volume of 10 ml/kg). At the beginning of the observations and before and after the treatments on days 1 and 2 whole body methane generation was detected. On day 2, after methane output measurements, the animals were anaesthetized with sodium pentobarbital (50 mg/kg i.p.). For instrumentation, the animals were placed in a supine position on heating pads, and the trachea and right jugular vein were cannulated to secure spontaneous breathing and *iv* administration of fluids and fluorescence dye, respectively. After a midline abdominal incision, intravital videomicroscopy was performed to examine the microcirculatory changes on the serosal surfaces of stomach, duodenum, jejunum, ileum and colon, respectively. Whole body methane detection was performed individually 24 h after the treatments (Figure 2).

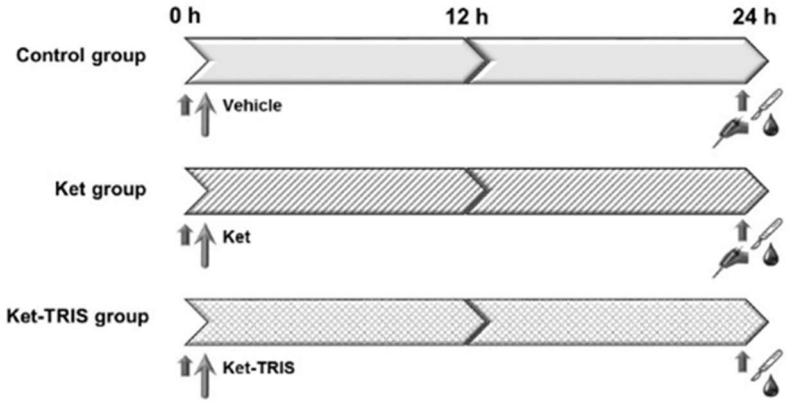

Figure 2. *Experimental protocol and timeline of Study 1/2*

3.1.4 Experimental protocol of Study 1/3: Connection between whole-body methane emission and TNBS-colitis induced GI microcirculatory changes with anti-inflammatory treatment.

In Study 1/3 (n=24) the control group (n=6) received enemas with a total volume of 0.25 ml containing 25% of ethanol (the solvent for TNBS). In groups 2, 3, and 4 (n=6, each) colitis was induced with a TNBS enema (40 mg/kg). In groups 3 and 4 Ket (Col+Ket; 0.56 mmol/kg, 20 mg/kg, in a volume of 10 ml/kg) or Ket-Tris conjugate (Col+Ket-Tris; 0.56 mmol/kg, (20 mg/kg, in a volume of 10 ml/kg), were gavaged to the animals 12 h after colitis induction. The animals in the control and the non-treated colitis groups were gavaged with the solvent for Ket (10 ml/kg buffered 0.11 M of potassium hydroxide). On day 2 (24 h after Ket or Ket-Tris treatments), the animals were anesthetized and surgery was performed. The animals were placed in a supine position on heating pads, the trachea and the right jugular vein were cannulated and after a midline abdominal incision. The lumen of the distal colon was exposed; then the mucosa was rinsed with saline to remove bowel content. In each group, *in vivo* histology of the colonic mucosa was performed to examine the changes in microvasculature. Whole body methane detection was performed individually 24 h after the treatments (Figure 3).

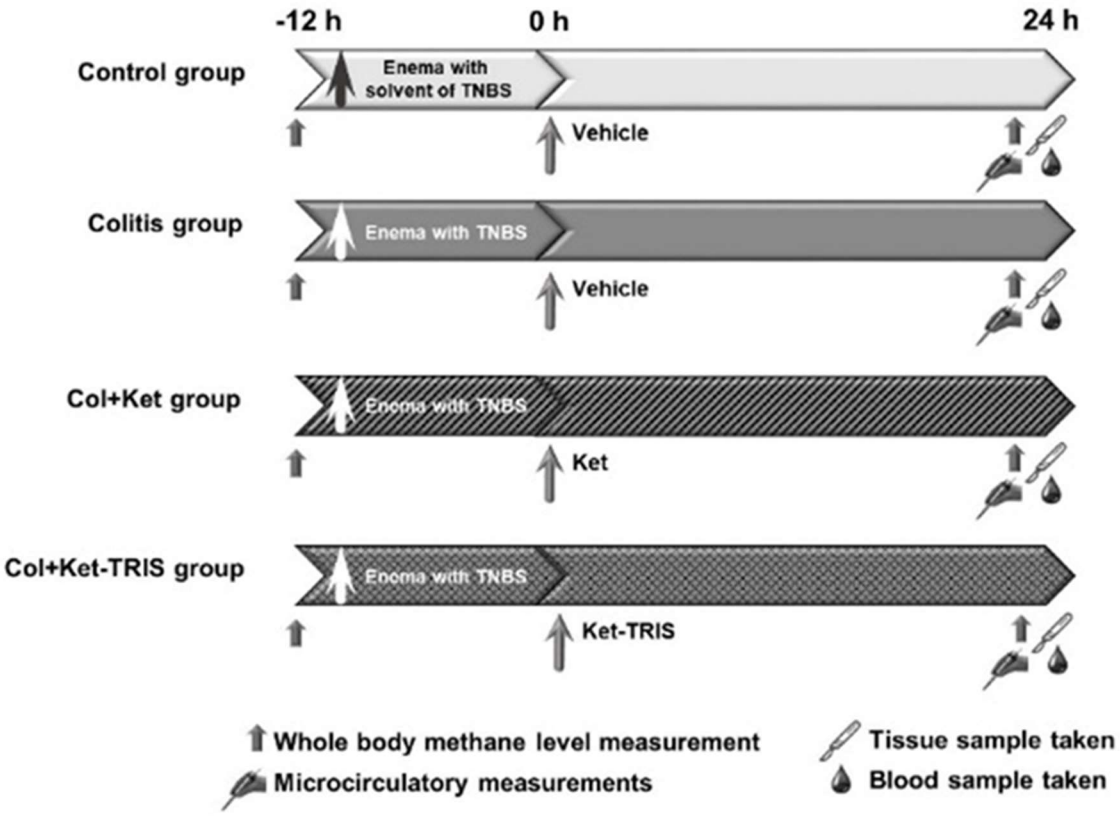

Figure 3. *Experimental protocol and timeline of Study 1/3*

3.2 Study 2: Diagnostic value of methane exhalation in a pig model of gradual, controlled hemorrhage

3.2.1 Animals

The experiments were performed on male outbred Vietnamese minipigs (n=6; 40±3 kg bw) in accordance with National Institutes of Health guidelines on the handling of and care for experimental animals and EU Directive 2010/63 on the protection of animals used for scientific purposes (approval number V/148/2013). The animals were kept in the animal house for acclimatization period of 7 to 10 days with natural circadian light and free access to water and food. Prior to the experiments the animals were fasted for 12 h with free access to tap water.

3.2.2 Surgical preparations

Male outbred Vietnamese minipigs (n=6; weighing 40±3kg) were used. Anesthesia was induced with a mixture of tiletamine zolepam (5 mg kg^{-1} im, Virbac, Carros, France) and xylasin (2 mg kg^{-1} im, Pordulab Pharma, Raamsdonksveer, The Netherlands). The animals were placed

in supine position on a warming pad with body temperature kept at 37.5±0.4 C°. After endotracheal intubation, mechanical ventilation was started with a tidal volume of 8-10 mL kg^{-1}, and the respiratory rate was adjusted to maintain the end-tidal pressure of carbon dioxide in the 35–45 mmHg range. Anaesthesia was maintained with a continuous infusion of propofol (6 mg kg^{-1} h^{-1} iv; Fresenius Kabi, Bad Homburg, Germany), midazolam (1.2 mg kg^{-1} h^{-1}; Torrex Chiesi Pharma, Vienna, Austria) and fentanyl (0.02 kg^{-1} h^{-1}; Richter Gedeon, Budapest, Hungary). Ringer's lactate (RL) infusion was administered at a rate of 10 ml kg^{-1} h^{-1} until bleeding was started. The depth of anaesthesia was regularly controlled by monitoring the jaw tone and the absence of interdigital reflex.

The left jugular vein was cannulated for fluid and drug administration, as was the left femoral artery for invasive monitoring of mean arterial pressure (MAP) (PICCO Plus; PULSION Medical Systems, Feldkirchen, Germany). The left carotid artery was cannulated for blood withdrawal. After median laparotomy, the superior mesenteric artery (SMA) was dissected free, and a flow probe (Transonic Systems Inc., Ithaca, NY, USA) was placed around it to measure SMA flow. The wound in the abdominal wall was then temporarily closed with clips.

3.2.3 Experimental protocol

After the surgical preparation, a 30-min stabilizing period was provided, followed by baseline measurements. Gradual bleeding was then started. The protocol was divided into seven steps with haemorrhage (T0–T7) followed by gradual fluid resuscitation in five steps (T8–T12), until 80% of the baseline MAP value was reached (Figure 4A). The total blood volume (BV) was set as 65 mL kg^{-1}, 5% of the estimated BV was withdrawn (129±8 mL) by the end of each bleeding step, and an equal volume of hydroxyethyl starch (HES; Voluven 6%, 130/0.4; Fresenius Kabi, Bad Homburg, Germany) was administered during each resuscitation step.

Every bleeding or resuscitation interval was started with microcirculatory recordings at the ileal mucosal and serosal surfaces and at the sublingual area. At each location, three, 20-sec video recordings were made. Following the intravital videomicroscopic investigations, MAP and SMA flow were recorded and finally blood samples were taken for lactate, total haemoglobin (tHb) and haematocrit (Hct) determinations. Methane values were continuously recorded throughout the observation period. At the end of the experiments the animals were sacrificed with an overdose of pentobarbital sodium (120 mg kg^{-1} iv; Sigma-Aldrich Inc, St. Louis, MO, USA). The timeline of measurement intervals is summarized in Figure 4B.

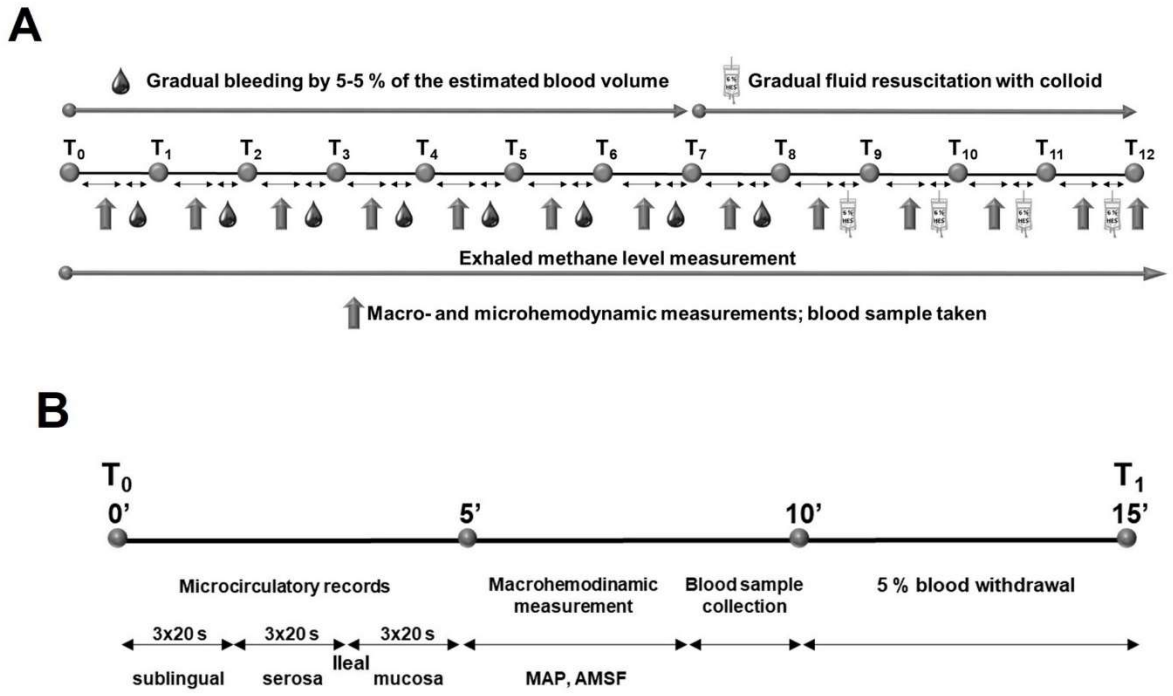

Figure 4. *Experimental protocol (**A**) and timeline of a measurement period during the experiment (**B**).*

3.3 In vivo measurements

3.3.1 Direct measurements of the microcirculation

In Study 1/1 and Study 2, the Cytocam-Incident Dark Field (IDF) imaging technique (CytoCam Video Microscope System, Braedius Medical, Huizen, the Netherlands) was used to visualize and evaluate the microcirculation. IDF imaging is optimized to visualize the haemoglobin-containing structures by illuminating the organ surface with linearly polarized light (Aykut et al, 2015).

In Study 2, the microcirculation of the ileal serosal and mucosal layers and the sublingual area were observed. In Study 1/1 and 1/3, the microcirculation of colon serosa were measured.

Images of empty bowel segment microcirculation and sublingual microcirculation were recorded in three, 20-sec, high-quality video clips per location by the same investigator, and records were saved as digital AVI-DV files to a hard drive. Optical magnification of 4x was used, to provide a 1.55 x 1.16 mm field of view. Every video clip was evaluated offline using analyzing software (AVA 3.0; Automated Vascular Analysis, Academic Medical Center, University of Amsterdam). The capillaries (with diameter less than 20 μm) were categorized by sight as capillaries with no flow, sluggish flow or continuous flow. The number of

intersections of capillaries with at least sluggish flow with three equidistant horizontal and three equidistant vertical lines was counted and was manually entered in the corresponding tool in the analyzing software to calculate the De Backer score (DBS). The microvascular flow index (MFI) was determined in four quadrants of a record according to the score system defined by the MFI evaluation tool in the analyzing software: no flow (1), sluggish flow (2) or continuous flow (3). The final MFI value of a record was the average for the MFI of the four quadrants. The microvascular heterogeneity index (HI) was calculated as the difference between the highest and lowest MFI of the three records divided by the mean MFI value of the same three videos (De Backer et al, 2007). Blinded evaluation was performed by two investigators (NV and AG).

In Study 1/2, the OPS imaging technique (Cytoscan A/R, Cytometrics, Philadelphia, PA, USA) was used for non-invasive visualization of the serosal microcirculation of the stomach, duodenum, jejunum, ileum or colon. This technique utilizes reflected polarized light at the wavelength of the isobestic point of oxy- and deoxyhaemoglobin (548 nm). As polarization is preserved in reflection, only photons scattered from a depth of 2–300 mm contributes to image formation. A 10x objective was placed onto the serosal surface of the stomach, and microscopic images were recorded with an S-VHS video recorder 1 (Panasonic AG-TL 700; Matsushita Electric Ind. Co. Ltd, Osaka, Japan). Quantitative assessment of the microcirculatory parameters was performed off-line by frame-to-frame analysis of the videotaped images. Red blood cell velocity (RBCV; μm/s) changes in the postcapillary venules were determined in three separate fields by means of a computer-assisted image analysis system (IVM Pictron, Budapest, Hungary).

3.3.2 Methane emission measurements

We employed a near-infrared laser technique-based PAS apparatus (Tuboly et al, 2013). PAS is a subclass of optical absorption spectroscopy that measures optical absorption indirectly via the conversion of absorbed light energy into acoustic waves due to the thermal expansion of absorbing gas samples. The amplitude of the generated sound is directly proportional to the concentration of the absorbing gas component. The gas sample passes through the photoacoustic cell, in which signal generation takes place, and a microphone then detects the photoacoustic signal produced. The gas samples were taken continuously from the exhalation outlet of the ventilator at a 150 mL min^{-1} rate during the experiments.

In Study 1, whole body methane level was measured. Gas samples were taken from the sampling chamber with an internal volume of 2510 cm^3. Before placing the animals into the chamber, the methane concentration of the gas in the chamber (room air) was determined and applied as the value of background methane concentration and it was subtracted from the value of the methane emission of the animals. Then the rat was placed in the chamber, it was sealed, and a sample of the chamber gas was analysed exactly 5 minutes later (a period of 5 min was sufficient for reliable and reproducible measurements in pilot studies). The rat was then removed, and the chamber was thoroughly ventilated with room air for 2 min between animals.

In Study 2, exhaled methane level was measured. The baseline exhaled methane values were determined, and the values were thereafter subtracted from the test values. The online-detected methane values were averaged for 60-sec periods to be identical with the parallel, 3 x 20-sec periods of the microcirculatory analyses.

3.4 In vitro measurements

3.4.1 Measurements of lactate level, total haemoglobin concentration and haematocrit

Changes in tHb, Hct and lactate concentration were analyzed with a cooximetry blood gas analyzer (Cobas b 123, Roche Ltd., Basel, Switzerland) from the arterial blood samples.

3.4.2 Tissue biopsies

Colon biopsies were kept on ice, then homogenized in phosphate buffer (pH 7.4), which contained 50 mM Tris-HCl (Reanal, Budapest, Hungary), 0.1 mM EDTA, 0.5 mM dithiotreitol, 1 mM phenylmethylsulfonyl fluoride, 10 μg/ml soybean trypsin inhibitor and 10 μg/ml leupeptin (Sigma-Aldrich GmbH, Germany). The homogenate was centrifuged at 4°C for 20 min at 24,000 g, and the supernatant was loaded into centrifugal concentrator tubes (Amicon Centricon-100; 100,000 MW cut-off ultrafilter).

3.4.3 Tissue xanthine oxidoreductase (XOR) activity

Colon biopsies were homogenized in phosphate buffer (pH 7.4) containing 50 mM Tris-HCl, 0.1 mM EDTA, 0.5 mM dithiotreitol, 1 mM phenylmethylsulfonyl fluoride, 10 μg ml^{-1} soybean trypsin inhibitor, and 10 μg ml^{-1} leupeptin. The homogenate was centrifuged at 4°C for 20 min at 24,000 g, and the supernatant was loaded into centrifugal concentrator tubes. XOR activity was determined in the ultrafiltered supernatant by a fluorometric kinetic assay based on

the conversion of pterine to isoxanthopterine in the presence (total XOR) or absence (XO activity) of the electron acceptor methylene blue (Beckman et al, 1989).

3.4.4 Tissue myeloperoxidase (MPO) activity

The myeloperoxidase (MPO) activity was measured in colon biopsies with the method developed by Kuebler et al. (1996). Briefly, the tissue was homogenized with Tris-HCl buffer (0.1 M, pH 7.4) containing 0.1 M polymethylsulfonyl fluoride to block tissue proteases and then centrifuged at 4°C for 20 min at 24,000 g. The MPO activities of the samples were measured at 450 nm (UV-1601 spectrophotometer; Shimadzu, Japan), and the data were referred to the protein content.

3.4.5 Tissue malondialdehyde (MDA) assay

MDA production is associated with oxidative damage of lipid membranes and thereby the degree of lipid peroxidation. MDA level was measured through the reaction with thiobarbituric acid reaction, and the values were corrected for the tissue protein content (Placer et al, 1966). The MDA concentration was determined on a standard curve (nmol/ml).

3.5 Statistical analysis

Data analysis was performed with a statistical software package (SigmaStat for Windows, Jandel Scientific, Erkrath, Germany). Normality of data distribution was analyzed with the Shapiro–Wilk test. The Friedman on ranks or one-way repeated measures analysis of variance (ANOVA) was applied within groups. Time-dependent differences from the baseline for each group were assessed with Dunn's method or the Bonferroni t-test. Differences among groups were analyzed with the Kruskal–Wallis one-way analysis of variance on ranks, followed by Dunn's method. Median values and 75^{th} and 25^{th} percentiles are provided in the figures; P values <0.05 were considered significant. Correlations between two variables were examined using Pearson's correlation coefficient (r); regression lines and 95% confidence intervals are provided in the figures.

4 RESULTS

4.1 Study 1: Effects of newly developed anti-inflammatory drugs on whole body methane emission

4.1.1 Study 1/1– Effects of TNBS

4.1.1.1 Changes in inflammatory mediators after colitis induction

On day 3, after colitis induction, significant elevation was demonstrated in the level of colonic MPO, XOR activity and MDA levels relative to the control group values (Figure 5ABC).

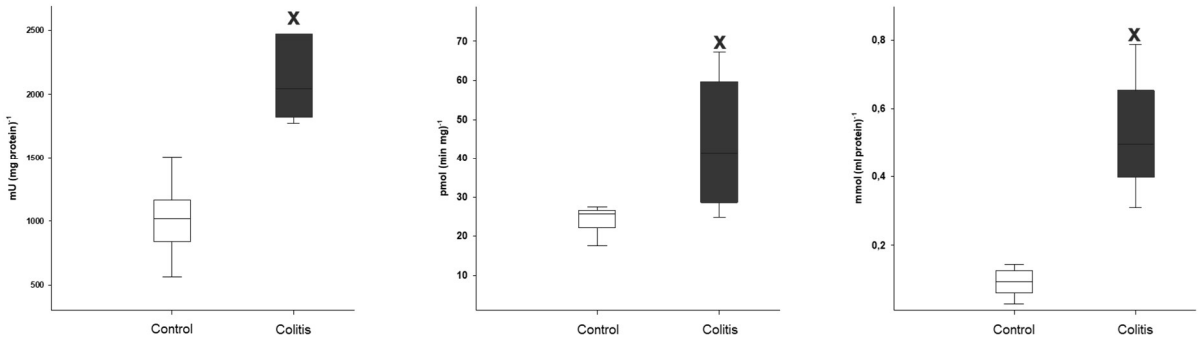

Figure 5. *Changes in colonic MPO activity (**A**), XOR activity (**B**) and MDA level (**C**) in the control (empty box) and colitis (black box) groups. The plots demonstrate the median (horizontal line in the box) and the 25th (lower whisker) and 75th (upper whisker) percentiles.* ^{x} *$P < 0.05$ between colitis vs control group.*

4.1.1.2 Changes in microcirculatory parameters

A significant increase was observed in the capillary flow index and DeBacker's score values in the colitis group on days 1, 2 and 3 of colitis relative to the control values (Figure 6AB).

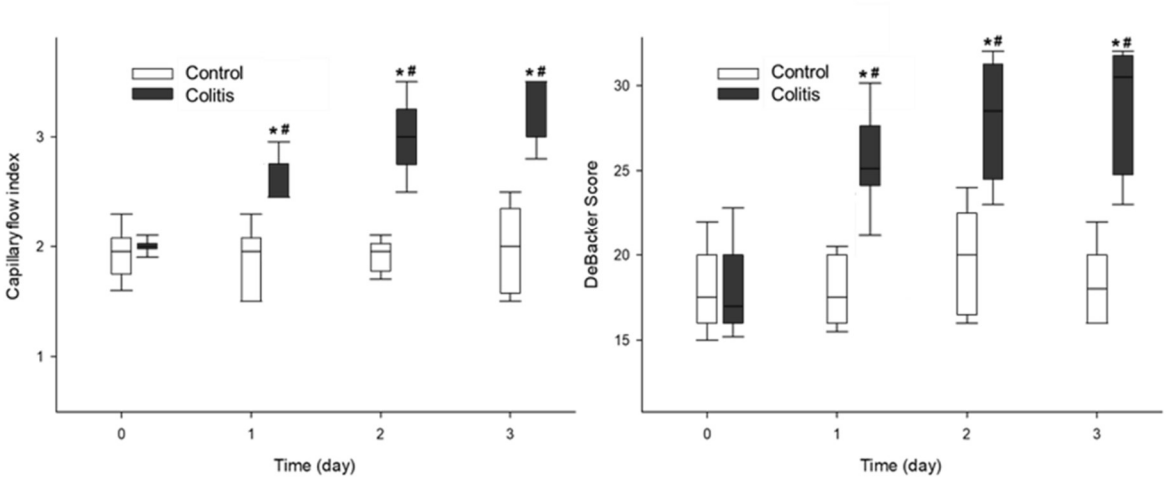

Figure 6. *Changes in capillary flow index (**A**) and De Backer score (**B**) in the control (empty box) and colitis (black box) groups. The plots demonstrate the median (horizontal line in the box) and the 25th (lower whisker) and 75th (upper whisker) percentiles.^{x} P < 0.05 between colitis vs control group.*

4.1.1.3 Changes in whole-body methane emission

Similarly, whole-body methane emissions were significantly elevated on days 2 and 3 after colitis induction in contrast to the control values and values of the control group (Figure 7).

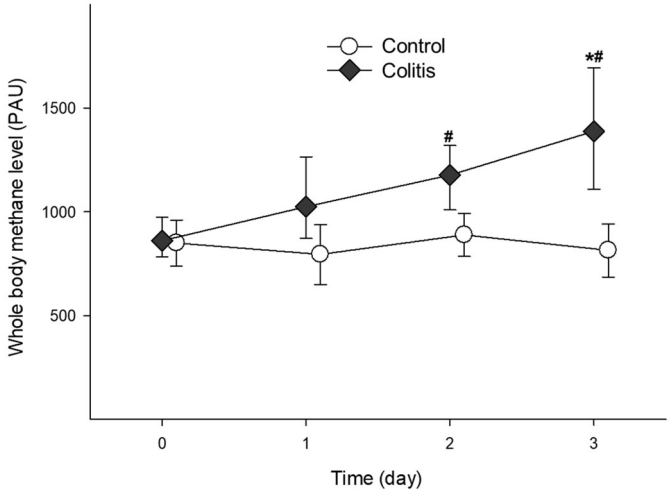

Figure 7. *Changes in whole methane emission in the control (white circle with solid line) and colitis (black diamond with solid line) groups. The plots demonstrate the median (horizontal line in the box) and the 25th (lower whisker) and 75th (upper whisker) percentiles.^{x} P < 0.05 between colitis vs control group.*

4.1.2 Study 1/2– Effects of Ket and Ket-Tris conjugate

4.1.2.1 In vivo detection of the microcirculation

RBCV of the mucosa was measured as a quantitative marker of GI microcirculatory condition. The RBCV in gastric serosa was significantly raised in the Ket-treated group as compared to the control group (Table 2), and a similar change was detected in the duodenum,

jejunum and ileum, but not in the colon. Baseline microcirculatory values were measured in the entire GI tract in the Ket-Tris-treated group (Table 1).

Table 1. *In vivo detection of the microcirculation in Study 2. The effects of Ket and Ket-Tris treatment on changes in red blood cell velocity [µm/s].* $^{a}p<0.05$ *between groups vs the control group;* $^{b}p<0.05$ *between the Ket-treated group vs the Ket-Tris-treated group.*

	Parameters	Control	Ket	Ket-Tris
Stomach	**Median**	**882**	**1084**^{a}	**763**^{b}
	25p; 75p	*779; 967*	*982; 1245*	*703; 876*
Duodenum	**Median**	**744**	**1084**^{a}	**676**^{b}
	25p; 75p	*694; 798*	*1015; 1229*	*536; 897*
Jejunum	**Median**	**762**	**1077**^{a}	**754**^{b}
	25p; 75p	*683; 824*	*960; 1267*	*679; 805*
Ileum	**Median**	**827**	**1012**^{a}	**781**^{b}
	25p; 75p	*742; 906*	*972; 1084*	*694; 864*
Colon	**Median**	**946**	**984**	**977**
	25p; 75p	*837; 1034*	*754; 1069*	*862; 1048*

4.1.2.2 Changes in whole-body methane emission

The whole-body methane level was measured before and 24 h after the treatments. In the control and Ket-Tris groups, no changes were detected at 24 h, while significant elevation was demonstrated 24 h after treatment in the Ket-treated group (Figure 8).

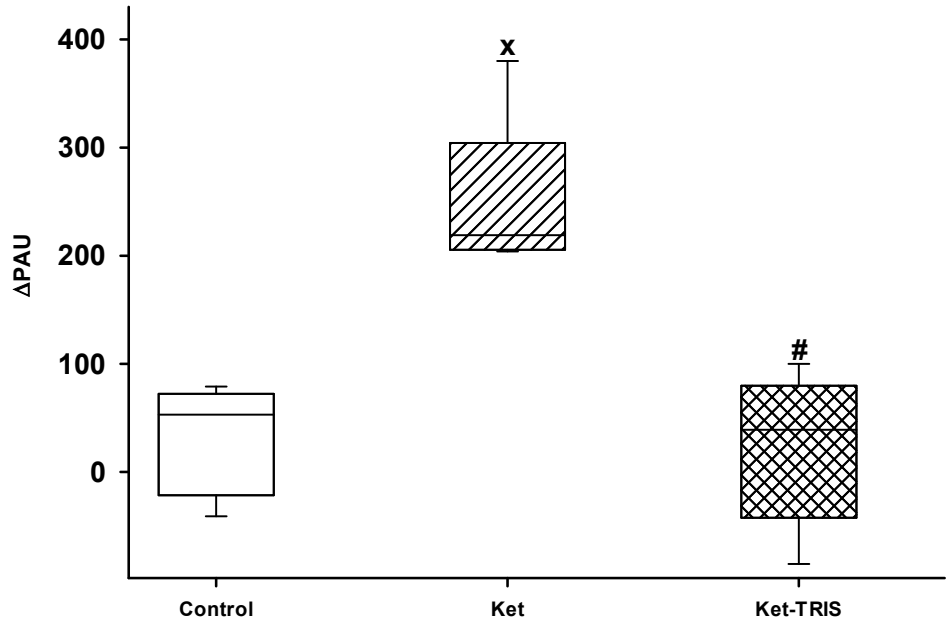

Figure 8. *Changes in whole-body methane emission; the difference between two successive measurement times is shown. Control (empty box), Ket-treated (striped box), Ket-Tris treated (checked box) groups. The plots demonstrate the median (horizontal line in the box) and the 25th (lower whisker) and 75th (upper whisker) percentiles. ^{x} P < 0.05 between groups vs control group, $^{\#}$ P < 0.05 between Ket-treated vs Ket-Tris treated groups.*

4.1.3 Study 1/3– Effects of Ket and Ket-Tris conjugate on TNBS induced colitis

4.1.3.1 In vivo detection of in the colon serosal microcirculation with in vivo microscopy

The RBCV in the colonic subserosa was significantly increased in colitis group as compared with the control group. Ket and Ket-Tris-treatment decreased the elevated RBCV by the end of the observation period (Figure 9).

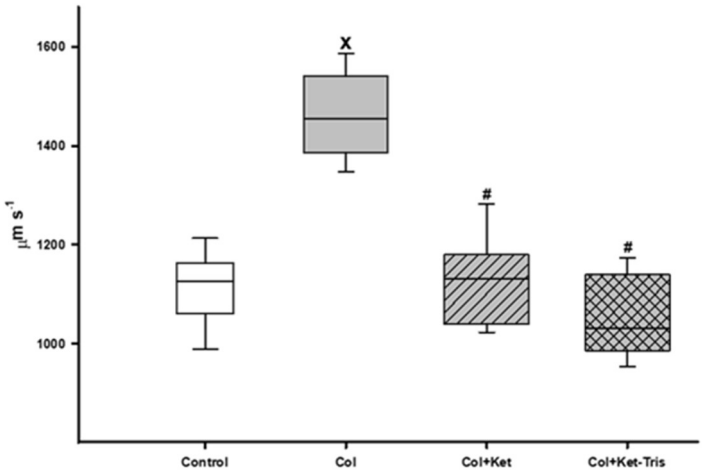

Figure 9. *Changes in serosal red blood cell velocity in the control (empty box), colitis (grey empty box), Ket-treated colitis (striped, grey box), Ket-Tris-treated colitis (checked grey box) groups. The plots demonstrate the median (horizontal line in the box) and the 25th (lower whisker) and 75th (upper whisker) percentiles. x p<0.05 between groups vs control group, # p<0.05 between non treated colitis group vs Ket or Ket-Tris treated groups.*

4.1.3.2 Changes of whole methane emission

Significant whole methane emission was detected after 24 h of colitis induction in colitis and Ket-treated colitis goups in contrast to the control group. The Ket-Tris-treatment did not result in a change in emission of methane (Figure 10).

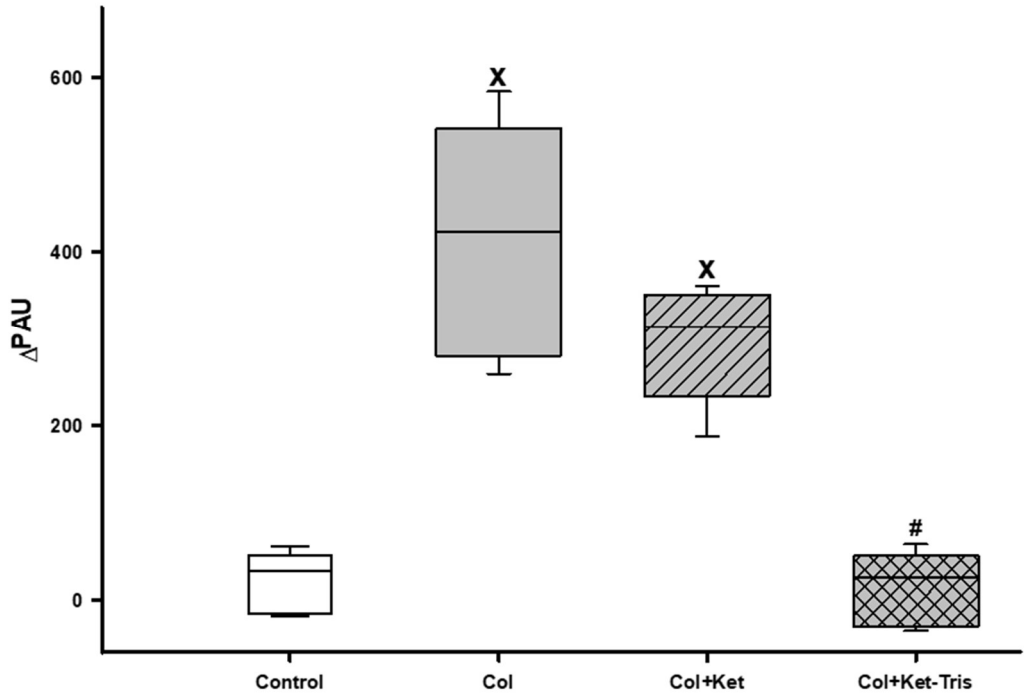

Figure 10. *Changes in whole methane emission in the control (empty box), colitis (grey empty box), Ket-treated colitis (striped, grey box), Ket-Tris-treated colitis (checked grey box) groups. The plots demonstrate the median (horizontal line in the box) and the 25th (lower whisker) and 75th (upper whisker) percentiles. x $p<0.05$ between groups vs control group, # $p<0.05$ between non treated colitis group vs Ket or Ket-Tris treated groups.*

4.2 Study 2: Diagnostic value of methane exhalation in a pig model of gradual, controlled hemorrhage

4.2.1 Systemic effects of gradual bleeding and resuscitation: changes in MAP

After the bleeding, MAP significantly decreased by T_3 (20% of blood loss) and remained significantly lower until the end of the hemorrhage phase. During the resuscitation period, it remained significantly lower than the control values until T_{10}, at which the volume of fluid replacement was equal to 15% of the estimated BV. By the end of the resuscitation phase, MAP reached 80% of the baseline value, as planned (Figure 11).

The plasma lactate level was increased significantly by T_6 (30% blood loss) and remained significantly higher compared with the baseline value until T_{11}. The bleeding and fluid resuscitation caused a continuous decrease in both tHb and Hct values. A significant difference from the baseline values was observed at T_6 in the case of both parameters. tHb was raised by more than 3 g dL^{-1} until the end of the hemorrhage phase (M=11.92; p25=9.7; p75=13.4 g dL^{-1} vs M=8.66; p25=7.43; p75=10.48 g dL^{-1}), which indicates severe bleeding (Table 2).

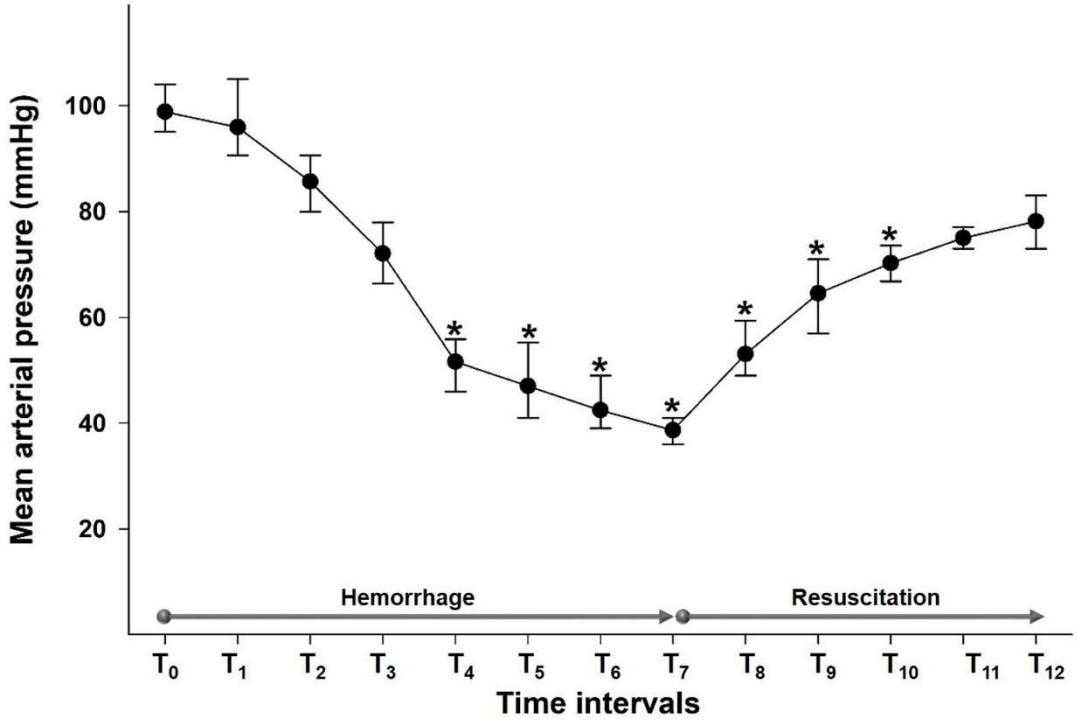

Figure 11. *Changes in mean arterial pressure (mmHg) during the hemorrhage and resuscitation phases. The plots demonstrate the median and the 25th (lower whisker) and 75th (upper whisker) percentiles. *p<0.05 within group vs. baseline values*

Table 2. *The effects of the hemorrhage and resuscitation phases on blood lactate [mmol L^{-1}], haematocrit (Hct) [%] and total haemoglobin (tHb) [g dL^{-1}]. The table demonstrates the median values and the 25th and 75th percentiles. * p<0.05 vs. baseline values.*

	Hemorrhage phase			
	Parameters	**Lactate**	**tHb**	**Hct**
T_0	**Median** *p25; p75*	**2.25** *1.97; 2.43*	**11.92** *9.7; 13.4*	**33.25** *27.75; 38.1*
T_1	**Median** *p25; p75*	**2.69** *2.2; 2.83*	**11.8** *9.45; 12.9*	**33.7** *28.25; 36.78*

T_2	**Median** *p25; p75*	**2.91** *2.73; 3.2*	**11.13** *9.0; 12.4*	**32.1** *26.9; 35.2*
T_3	**Median** *p25; p75*	**3.11** *2.77; 3.5*	**11.04** *9.02; 12.02*	**31.4** *25.7; 33.8*
T_4	**Median** *p25; p75*	**3.675** *3.438; 4.03*	**10.58** *8.8; 11.45*	**29.89** *25.5; 32.68*
T_5	**Median** *p25; p75*	**4.41** *4.27; 4.53*	**10.36** *8.55; 11.3*	**29.1** *24.9; 31.6*
T_6	**Median** *p25; p75*	**5.42 *** *4.65; 6.05*	**10.11 *** *8.28; 10.85*	**26.1 *** *23.38; 29.63*
T_7	**Median** *p25; p75*	**6.71 *** *5.88; 7.3*	**8.66 *** *7.43; 10.48*	**23.68 *** *20.9; 28.82*
		Resuscitation phase		
T_8	**Median** *p25; p75*	**6.33 *** *5.63; 7.0*	**7.99 *** *7.05; 10.23*	**21.97 *** *19.45; 27.97*
T_9	**Median** *p25; p75*	**5.4 *** *5.13; 6.1*	**7.5 *** *6.58; 9.68*	**20.56 *** *18.57; 26.2*
T_{10}	**Median** *p25; p75*	**4.65 *** *4.425; 5.4*	**7.29 *** *6.6; 8.98*	**18.8 *** *16.55; 24.0*
T_{11}	**Median** *p25; p75*	**4.418 *** *3.9; 4.85*	**6.9 *** *5.85; 8.2*	**17.38 *** *15.43; 21.88*
T_{12}	**Median** *p25; p75*	**3.95** *3.55; 4.85*	**6.75 *** *5.7; 7.87*	**16.37 *** *14.4; 20.77*

4.2.2 Mesenteric macrohemodynamics

The SMA flow decreased continuously during the hemorrhage phases. An early, significant drop was already noted at a 5% loss (T_1) of the estimated BV. After fluid resuscitation, the MAP started to increase steeply and reached its peak value at the second resuscitation step at T_8. During the following parts of the resuscitation phase, it decreased gradually to the level of the baseline values (Figure 12A).

4.2.3 Changes in exhaled methane levels

The average for baseline exhaled methane was 60.9–90.1 ppm, which corresponds to the higher range of values measured in methane-producing humans (Levitt et al, 2006). The individual baseline data were subtracted from the test values to increase the comparability of measurements even in the case of larger individual variances (Szűcs et al, 2019).

The exhaled methane concentration decreased significantly after 5% blood loss, already at T_1, similarly to the SMA flow changes. After resuscitation was started, breath methane level rapidly increased to a significantly higher level than the baseline and reached a peak after a fluid volume equal to 10% of estimated BV, administered at T_8 period (Figure 12B).

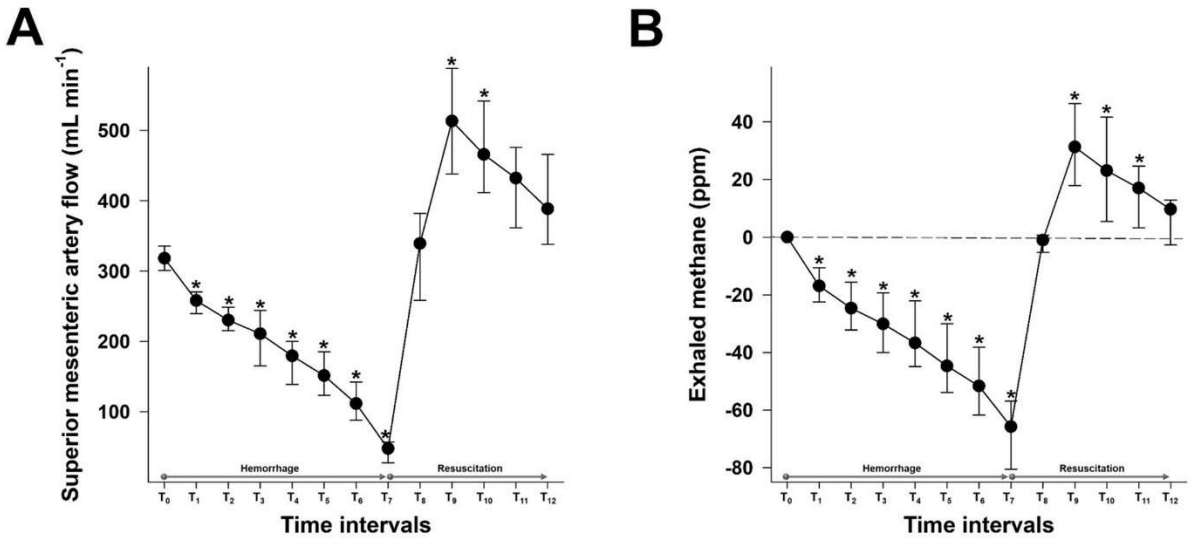

Figure 12. *Changes in the superior mesenteric artery flow (mL min^{-1}) (**A**) and exhaled methane levels (ppm) (**B**) during the hemorrhage and resuscitation phases. The plots demonstrate the median and the 25th (lower whisker) and 75th (upper whisker) percentiles. *p<0.05 within group vs. baseline values.*

4.2.4 Changes in sublingual and ileal microcirculation

The DBS values decreased significantly as the bleeding progressed. The serosal DBS was lower than the baseline value from a 10% blood loss (T_2). This was followed by a deterioration of mucosal DBS from the loss of 20% of estimated BV (T_4), while the decrease of DBS in the sublingual area was statistically significant from a 25% blood loss only (T_5). Moreover, the sublingual DBS was significantly higher than the values in the ileal regions from T_5 to T_7, which marks the end of the hemorrhage phase and a loss of 35% of BV. When fluid resuscitation started, the mucosal DBS increased rapidly and was significantly higher as compared to the serosal and sublingual values after fluid replacement with a volume equal to 5% of BV (T_8), reaching the highest value at T_{10}. The serosal DBS values increased more gradually with a maximum at T_{12} (Figure 13A).

Bleeding caused a decrease in the MFI in all three locations, and the first to reach significance was the MFI in the sublingual area at T_3. This was followed by a significant decrease in serosal MFI from T_4 and in mucosal MFI from T_5. The fluid resuscitation resulted

in a significant improvement of the MFI in all investigated locations. Sublingual MFI was significantly higher than the MFI in the ileal mucosa and serosa from T_{10} (Figure 13B).

The heterogeneity of the microcirculation increased during the hemorrhage phase as shown by the HI. The most important difference between the sublingual and ileal regions is that while the sublingual HI was restored during resuscitation, the HI in both the ileal mucosa and serosa remained significantly higher compared to the baseline and the sublingual values until the end of the experiments (Figure 13C).

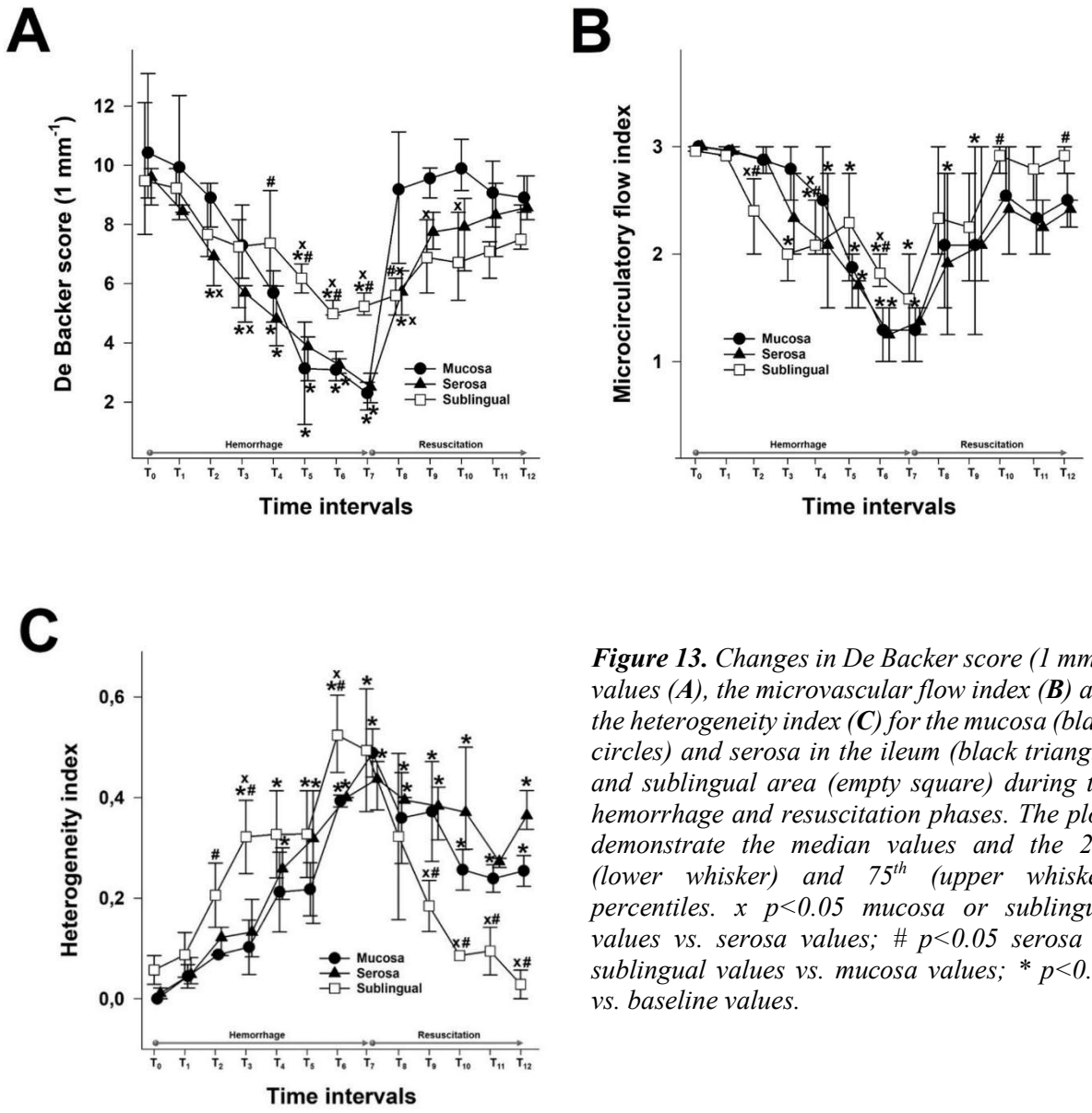

Figure 13. *Changes in De Backer score (1 mm^{-1}) values (**A**), the microvascular flow index (**B**) and the heterogeneity index (**C**) for the mucosa (black circles) and serosa in the ileum (black triangle) and sublingual area (empty square) during the hemorrhage and resuscitation phases. The plots demonstrate the median values and the 25th (lower whisker) and 75th (upper whisker) percentiles. x $p<0.05$ mucosa or sublingual values vs. serosa values; # $p<0.05$ serosa or sublingual values vs. mucosa values; * $p<0.05$ vs. baseline values.*

4.2.5 Link between changes in exhaled methane concentration and mesenteric macro- and microperfusion

We compared the changes in the exhaled methane concentration during the hemorrhage and resuscitation phases with SMA flow data. In the hemorrhage phase, a significant correlation was found (r=0.82; Figure 14A) and a significant relation could be demonstrated in the resuscitation phase as well (r=0.79; Figure 14B).

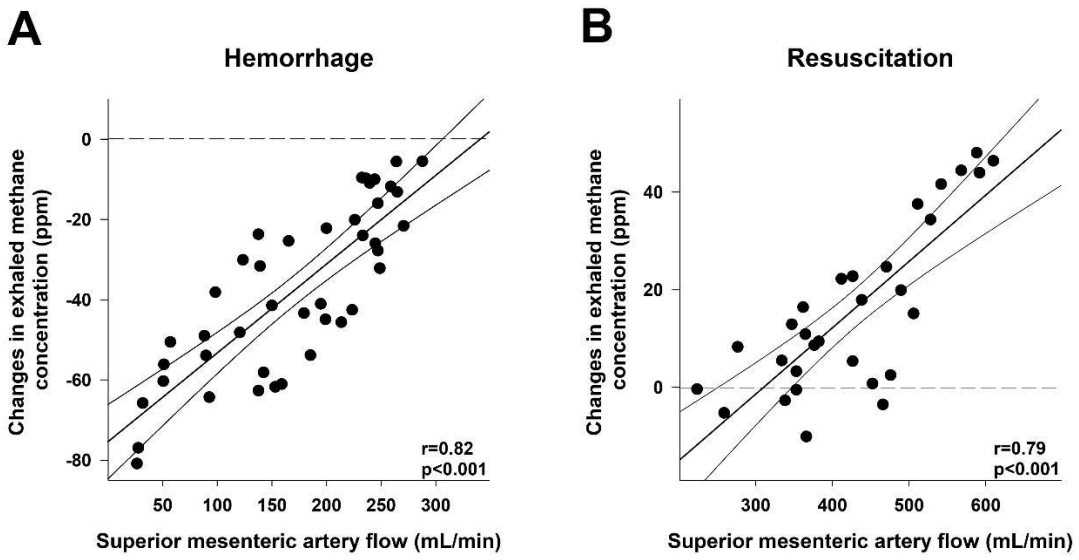

Figure 14. *Correlation between AMSF and changes in exhaled methane concentration during the hemorrhage (**A**) and resuscitation phases (**B**). The plot demonstrates the regression line (gray line), corresponding values (black scatters), **r** values as an indicator of the strength of the linear correlation and p significance values.*

When the possible links between the changes in exhaled methane levels and the DBS values of the two components of the ileal microcirculation during the hemorrhage and resuscitation were investigated, the DBS in the serosa correlated significantly with the exhaled methane values during bleeding (r=0.79; Figure 15A) and fluid resuscitation (r=0.66; Figure 15B). Similarly, a significant correlation was present in the case of the mucosal DBS values in both the hemorrhage (r=0.82; Figure 15C) and resuscitation phases (r=0.72; Figure 15D).

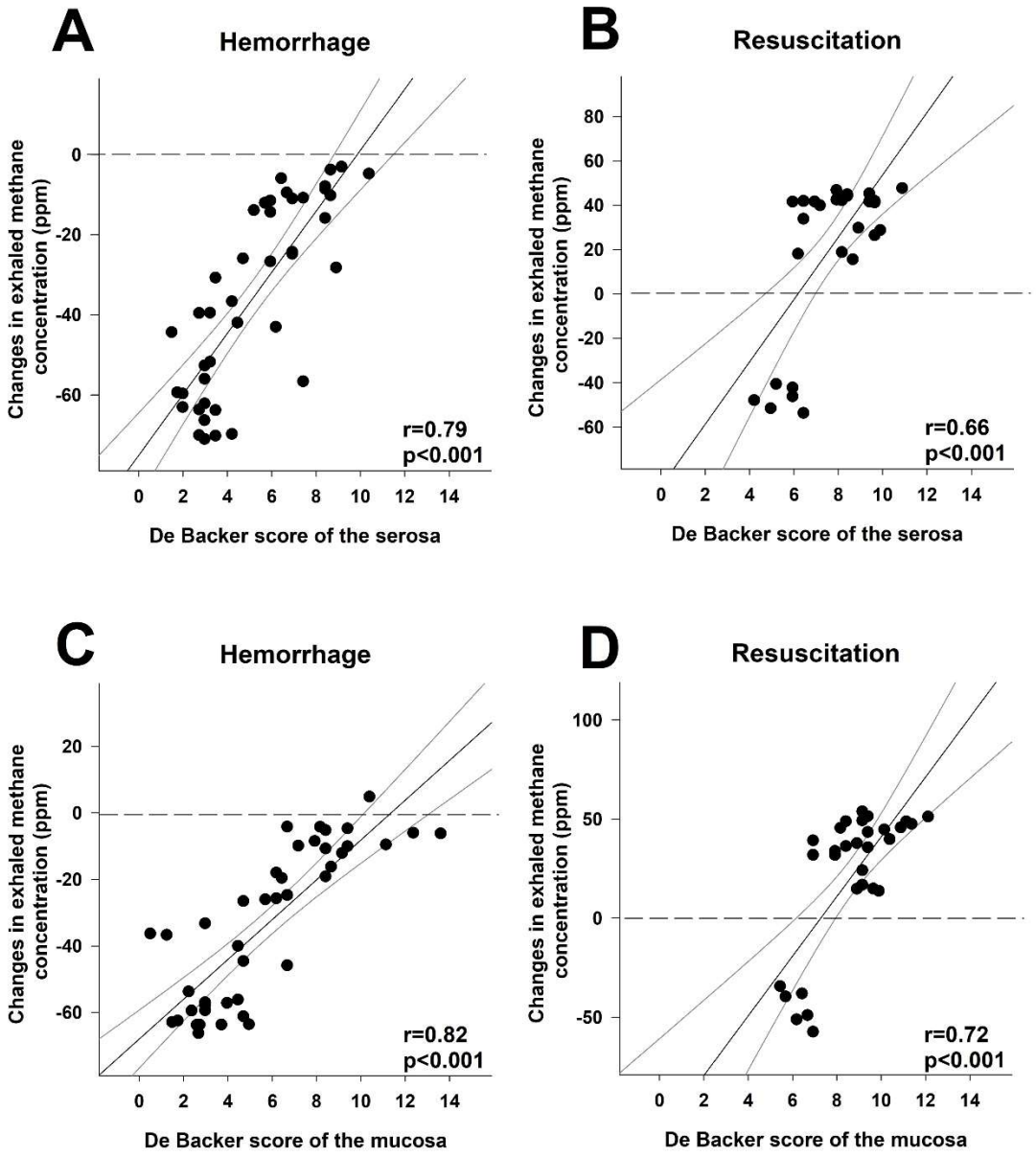

*Figure 15. Correlation between the De Backer score for the serosa (**A, B**) or mucosa (**C, D**) and changes in exhaled methane concentration during the hemorrhage and resuscitation phases. The plot demonstrates the regression line (gray line), corresponding values (black scatters), **r** values as an indicator of the strength of the linear correlation and p significance values.*

Phases are shown to demonstrate the changes in exhaled methane concentrations and the DBS of ileal mucosa on an original methane registration curve of a single animal and the simultaneous changes in the mucosal DBS in the same animal during hemorrhage and resuscitation (Figure 16).

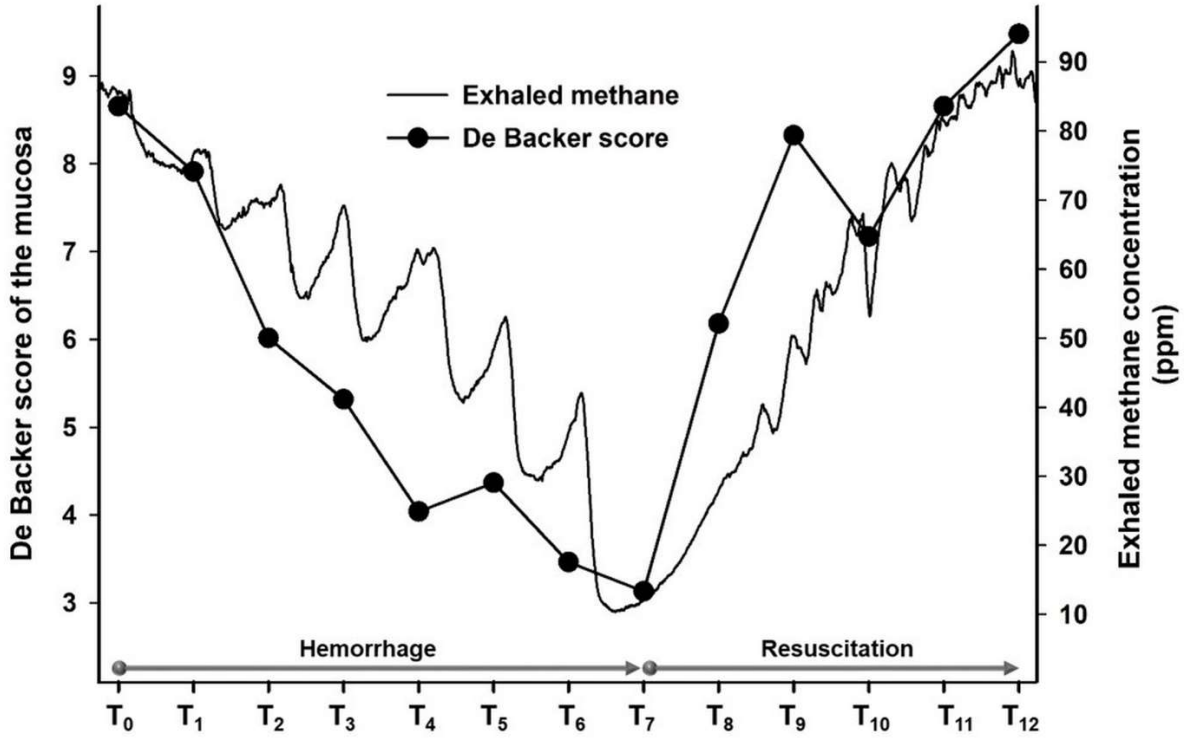

Figure 16. *Original tracings representing changes in exhaled methane levels (continuous black line) and the De Backer score for ileal mucosa (black circles) of an individual animal.*

4.2.6 Correlations between sublingual and ileal mucosal or serosal microcirculation

Significant correlations were detected during the hemorrhage phase between the sublingual DBS and the serosal or mucosal DBS values (r=0.74 and r=0.66, respectively; Figure 17AB).

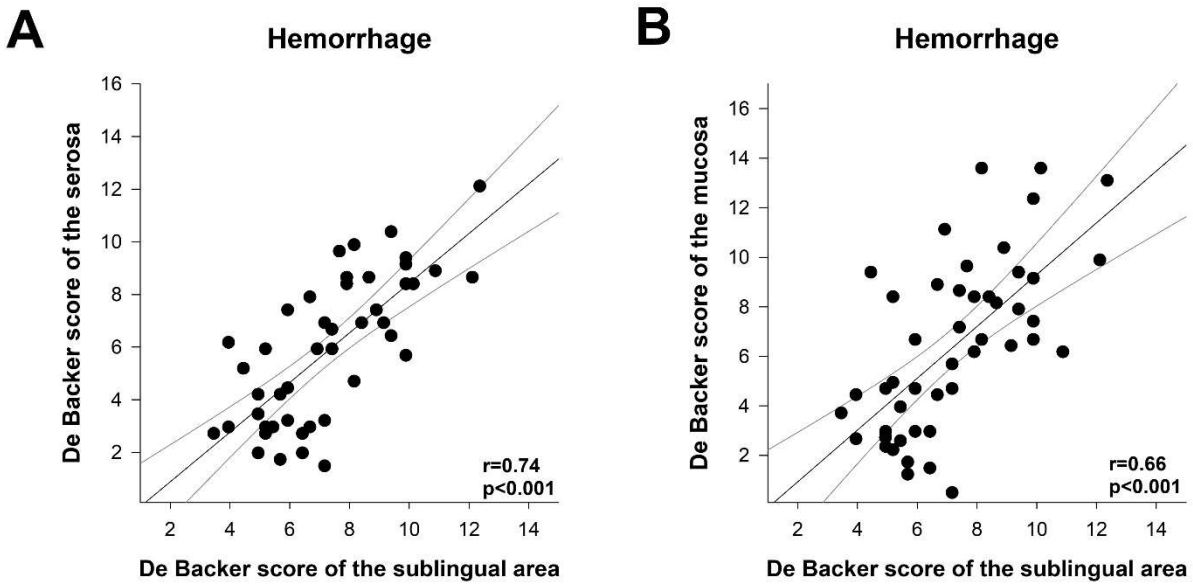

Figure 17. *Correlation between the De Backer score for the serosa (**A**) or mucosa (**B**) and the De Backer score for the sublingual area during the hemorrhage phase. The plot demonstrates the regression line (gray line), corresponding values (black scatters), **r** values as an indicator of the strength of the linear correlation and p significance values.*

5 DISCUSSION

The primary objective of Study 1 was to examine the relationship between whole-body methane emission and colonic mucosal inflammation and colonic and small intestinal serosal microcirculation in experimental rat models. To achieve this, we employed first a standardized method for inducing inflammatory stress, specifically TNBS-induced experimental colitis, which is known to result in varying degrees of mucosal damage across different regions of the GI tract. In this experimental setup, the administration of a TNBS enema resulted in significant mucosal injury, accompanied by elevated activities of inflammatory enzymes, hyperemic microcirculatory reaction in the colon and an increased whole-body methane emission. Another objective of this protocol was to assess the link between methane production and enzymes or markers of the oxidative stress in a condition characterized by intestinal inflammation. The inflammatory response was characterized by hyperemic microcirculation, and the activation of XOR, a key enzyme involved in ROS generation. Moreover, whole-body methane emissions were significantly increased in comparison to vehicle-treated control animals. Building upon our current findings and the hallmark indicators of inflammation, we propose that the elevated methane output observed in this in vivo model is attributable, in part, to the inflammatory hyperemia affecting the large intestine and, in part, to localized ROS generation within the bowel wall.

In a subsequent experimental model, we investigated drug-induced microcirculatory responses within the GI tract. To this end, we administered Ket and Ket-Tris -original and chemically modified non-steroidal anti-inflammatory drugs (NSAIDs) - based on the hypothesis that the two compounds would exert distinct effects on microcirculation. A novel aspect of our study lies in the real-time monitoring of whole-body methane emissions, conducted in a sufficiently large cohort of experimental animals to ensure statistical robustness. It is widely recognized that the majority of methane produced in the mammalian intestine is excreted via the lungs, leading to the utilization of breath testing as a diagnostic tool for certain GI conditions. However, due to its physicochemical properties, methane is evenly distributed across membrane barriers and can traverse the mucosal surfaces freely. Consequently, its production is reflected not only in exhaled air but also in its passage through various body surfaces (Nose et al, 2005). Moreover, recent studies have established a correlation between the carrier capacity of GI microcirculation and the concentration of methane in exhaled air (Szűcs et al, 2019). Our analytical approach, utilizing specific PAS detection, effectively captured both

the dynamics of methane production and the overall profile of net methane generation across various groups of unrestrained animals (Tuboly et al, 2013). In this experimental setup, we observed a significantly higher whole-body methane output following oral administration of Ket, whereas no such change was noted with the administration of the Ket-Tris conjugate.

Traditionally, GI methane formation has been understood as the enzymatic product of the metabolism of strictly anaerobic methanogenic archaea, a distinct class of prokaryotes (Conrad 2009; Ellermann et al, 1988). However, a substantial body of evidence accumulated over the past decade has unequivocally demonstrated that eukaryotes can directly release methane in the absence of microbial activity and in the presence of oxygen (Boros and Keppler, 2019). More recently, compelling evidence has emerged indicating that biotic methane formation occurs across all multicellular life forms, even under aerobic conditions (Keppler et al, 2006; Wang et al, 2021). Previous studies have shown that methane can be generated in chemical model systems when methyl group-containing compounds are incubated with ferric iron, ascorbate, and hydrogen peroxide in the absence of enzymatic activity (Ghyczy et al, 2003). Ernst et al. (2022) demonstrated that ROS-induced methyl radicals, derived from organic compounds containing sulfur- or nitrogen-bonded methyl groups, serve as key intermediates leading to methane production in all eukaryotes, including human cell lines (Liu and Zhang, 2022). Although the biological significance of this reaction remains incompletely understood, the cumulative data suggest that methane excretion in the breath of mammals reflects intestinal bacterial fermentation, alongside an unknown and variable contribution from de novo generation induced by metabolically active target cells under conditions of oxidative stress (Tuboly et al, 2013; Ernst et al, 2022). This interpretation implies that in Study 1/2 the signal intensities associated with Ket-Tris-linked microcirculatory responses are significantly lower than those observed following the administration of the original Ket molecule.

The previously discussed role of ROS in the development of gastric and intestinal hyperemia also helps explain the observed alterations in methane emissions following treatment with Ket or Ket-Tris during TNBS-induced colitis. The increased methane production in the Ket-treated colitis group, contrasted with the marked reduction in methane output after Ket-Tris administration - as demonstrated in Study 1/3 - suggests a more potent anti-inflammatory effect exerted by Ket-Tris (Ugocsai et al, 2023). Consequently, the influence of the Ket-Tris conjugate may exert a more pronounced effect on colonic microcirculation, leading to reduced methane emissions. Thus, we propose that real-time monitoring of exhaled methane levels may serve as an effective method for examining and tracking ROS-driven mucosal inflammatory

processes within the GI system, as well as for evaluating the effects of various therapeutic interventions, at least in rodent models.

The limitations of this study warrant discussion, particularly given the relatively short follow-up period employed in this complex experimental scenario. Further research is essential to elucidate the precise intracellular and molecular mechanisms underlying mucosal defense and repair in relation to the protective effects of Tris conjugation. Additional investigations into gene signatures and transcriptional responses, as well as relevant cytotoxic events affecting the mucus-bicarbonate barrier and cyclooxygenase-pathway markers, could provide further insights following compound treatments. In conclusion, the results presented in this thesis substantiate the specific protective effect of Tris in safeguarding the GI tract from NSAID-induced damage. In these experiments, net methane production was observed, with whole-body methane output closely correlating with the inflammatory status and microcirculation of the GI mucosa. In animals treated with Ket-Tris, methane production was maintained at levels comparable to those of the sham-operated group, suggesting that methane may serve as an alarm signal during the onset of pro-inflammatory responses, as well as a potential indicator of anti-inflammatory interventions aimed at modulating such events.

In Study 2, we employed continuous, real-time detection of exhaled methane concentration to elucidate the relationship between this biomarker and the macro- and microvascular components of the mesenteric circulation during and following hemorrhagic events. Our findings indicate that alterations in SMA flow occurred prior to changes in systemic hemodynamic parameters and Htc levels. Furthermore, the fluctuations in exhaled methane concentrations closely mirrored the modifications observed in mesenteric circulation. Based on these observations, we propose that monitoring exhaled methane may serve as an effective early warning tool for the identification of internal hemorrhage. Additionally, the assessment of exhaled methane levels can provide valuable insights into the status of the microcirculatory components of the mesenteric region during episodes of bleeding. This method is also capable of detecting rapid changes during the initial phase of fluid resuscitation.

The methane breath test is an established diagnostic tool for various GI disorders. In clinical laboratory practice, breath methane levels are typically assessed using a lactulose test, wherein breath samples are collected in gas-tight bags and subsequently analyzed via GC. This analysis is conducted using detectors such as flame ionization, thermal conductivity, or mass spectrometry (Costello et al, 2013). It is important to note that the sampling frequency of these conventional methods is inherently limited. In contrast to the GC technique, our approach

utilizes PAS, which allows for real-time monitoring of methane concentration changes with a sensitivity threshold of less than 1 ppm, compared to the 3 ppm sensitivity threshold of currently available GC instruments. This methodology enables the dynamic assessment of exhaled methane concentrations even within single breath sample analyses (Tuboly et al, 2013). For our investigation, we employed an anesthetized acute pig model to simulate a controlled hemorrhagic event. The model involved a gradual and relatively low rate of BV loss (5% per step), culminating in a severe hemorrhage followed by a controlled, gradual, and restricted fluid resuscitation aimed at maintaining MAP at 80% of baseline levels. The total BV loss was established at 35%, resulting in an approximate decrease of 3 g dL^{-1} in tHB, thereby confirming the severity of the hemorrhagic event. This low rate of blood loss facilitated a high temporal resolution, allowing for seven measurement intervals during the hemorrhage phase and five intervals until the target MAP was achieved during the resuscitation phase. We selected HES as the resuscitation fluid, anticipating that it would induce significant macrohemodynamic changes while also having the potential to restore intestinal microcirculation (Wu et al, 2015).

As anticipated, the blood flow in the SMA was significantly affected at an early stage, exhibiting a notable decrease following the withdrawal of 5% of total BV. This reduction in SMA blood flow was closely mirrored by corresponding changes in exhaled methane concentration, which exhibited similar dynamics. Significant alterations in the DBS of both the serosal and mucosal components of the ileal microcirculation were observed slightly later, occurring after 10% and 20% blood loss, respectively. The observed disparity between mesenteric macro- and microcirculation may be attributed to a potential autoregulatory mechanism governing mesenteric microperfusion (Pestel et al, 2010). Furthermore, the temporal delay between changes in the mucosal and serosal microcirculation may be explained by the phenomenon of microcirculatory redistribution, which prioritizes the oxygenation of the mucosal layer at the expense of reduced perfusion to the serosal layer (Hiltebrand et al, 2003). The earlier decline in exhaled methane levels may suggest a reduction in the absolute volume of perfused blood, without a corresponding decrease in perfused capillary density.

At the onset of the resuscitation phase (T8–T9), a marked increase in SMA blood flow, mucosal DBS, and exhaled methane levels was observed. However, by the conclusion of the experimental protocol, both exhaled methane concentrations and SMA flow values exhibited a decline, with no significant differences detected when compared to baseline values. Throughout the resuscitation phase, the DBS of both the mucosal and serosal regions remained stable, with no reductions noted during the final two measurement intervals. Despite these observations, the

HI demonstrated an increase by the end of the hemorrhage phase and remained elevated throughout the entirety of the resuscitation phase. This finding suggests that microcirculatory perfusion was not fully restored following fluid resuscitation, which may account for the observed decrease in methane levels subsequent to the initial peak.

The microcirculation of the sublingual region is frequently studied due to its suitability for non-invasive assessment, with the assumption that alterations in this area may reflect the microcirculatory status of more distal GI regions, such as the ileum. Previous research has demonstrated a relationship between tissue carbon dioxide pressure in the sublingual area and changes in small intestinal microcirculation during models of hemorrhagic shock and fluid resuscitation (Palágyi et al, 2015). In Study 2, we were unable to establish a correlation between sublingual microcirculation and the serosal or mucosal components of ileal microperfusion during the resuscitation phase. This finding underscores the methodological differences between the two assessment techniques. While investigations of the sublingual area can capture GI microcirculatory changes over a broader timeframe, they are not influenced by increased sampling frequency due to the inherent inertia between the sublingual and more distal microcirculatory regions. Conversely, the dynamics of changes in exhaled methane concentrations closely mirrored those observed in mesenteric circulation. Real-time monitoring of exhaled methane levels effectively captured the rapid changes occurring during the early phase of resuscitation.

Alterations in exhaled methane concentration may serve as an early indicator of bleeding and can reflect changes in mesenteric perfusion throughout the course of hemorrhage and subsequent resuscitation. The diagnostic value of this method appears to be comparable to that of monitoring the sublingual microcirculatory area. Consequently, exhaled methane measurement could represent a valuable, non-invasive adjunctive tool in clinical scenarios where hemorrhagic complications are anticipated. Furthermore, even in its current implementation, this technique may enhance the acquisition of additional insights regarding mesenteric circulation within experimental frameworks.

6 SUMMARY OF NEW FINDINGS.

1. Changes in whole-body methane emissions reflected alterations in small intestinal microcirculatory parameters induced by TNBS and
2. drug (NSAID) administration.
3. Whole-body methane production increased in parallel with GI inflammatory activation in TNBS-induced colitis. Therefore, real-time measurement of methane emission may serve as a non-invasive tool to estimate the progression of GI inflammation and monitor the effects of therapeutic interventions.
4. In a large animal model of controlled, gradual haemorrhage, exhaled methane levels showed a significant correlation with SMA blood flow as well as ileal mucosal and serosal microcirculation. Moreover, methane levels responded earlier to changes in SMA flow compared to sublingual microcirculation.
5. During the resuscitation phase, rapid shifts in small intestinal microcirculation were mirrored by changes in exhaled methane levels, whereas sublingual microcirculation failed to reflect these dynamic alterations.

7 REFERENCES

1. Aykut G., Veenstra G., Scorcella C., İnce C., Boerma E. Cytocam-IDF(incident dark field illumination) imaging for bedside monitoring of the microcirculation. *Intensive Care Medicine Experimental* 2015;3(1). https://doi.org/10.1186/s40635-015-0040-7
2. Beckman J., Parks D., Pearson J., Marshall P., Freeman B. A sensitive fluorometric assay for measuring xanthine dehydrogenase and oxidase in tissues. *Free Radical Biology and Medicine* 1989;6(6):607-615. https://doi.org/10.1016/0891-5849(89)90068-3
3. Boerma E., Voort P., Spronk P., Ince C. Relationship between sublingual and intestinal microcirculatory perfusion in patients with abdominal sepsis. *Critical Care Medicine* 2007;35(4):1055-1060. https://doi.org/10.1097/01.ccm.0000259527.89927.f9
4. Bond J., Engel R., Levitt M. Factors influencing pulmonary methane excretion in man. *The Journal of Experimental Medicine* 1971;133(3):572-588. https://doi.org/10.1084/jem.133.3.572
5. Boros M. and Keppler F. Methane production and bioactivity-a link to oxido-reductive stress. *Frontiers in Physiology* 2019;10. https://doi.org/10.3389/fphys.2019.01244
6. Boros M., Ghyczy M., Érces D., Varga G., Tőkés T., Kupai K. et al. The anti-inflammatory effects of methane. *Critical Care Medicine* 2012;40(4):1269-1278. https://doi.org/10.1097/ccm.0b013e31823dae05
7. Boros M., Tuboly E., Mészáros A., Amann A. The role of methane in mammalian physiology—is it a gasotransmitter? *Journal of Breath Research* 2015;9(1):014001. https://doi.org/10.1088/1752-7155/9/1/014001
8. Bozóki Z., Pogány A., Szabó G. Photoacoustic instruments for practical applications: present, potentials, and future challenges. *Applied Spectroscopy Reviews* 2011;46(1):1-37. https://doi.org/10.1080/05704928.2010.520178
9. Conrad R. The global methane cycle: recent advances in understanding the microbial processes involved. *Environmental Microbiology Reports* 2009;1(5):285-292. https://doi.org/10.1111/j.1758-2229.2009.00038.x

10. Costello B., Ledochowski M., Ratcliffe N. The importance of methane breath testing: a review. *Journal of Breath Research* 2013;7(2):024001. https://doi.org/10.1088/1752-7155/7/2/024001

11. De Backer D., Hollenberg S., Boerma E., Goedhart P., Büchele G., Ospina-Tascón G. et al. How to evaluate the microcirculation: report of a round table conference. *Critical Care* 2007;11(5). https://doi.org/10.1186/cc6118

12. De Backer D., Ortiz J., Salgado D. Coupling microcirculation to systemic hemodynamics. *Current Opinion in Critical Care* 2010;16(3):250-254. https://doi.org/10.1097/mcc.0b013e3283383621

13. Dubin A., Pozo M., Casabella C., Murias G., Moseinco M., Edul V. et al. Increasing arterial blood pressure with norepinephrine does not improve microcirculatory blood flow: a prospective study. *Critical Care* 2009;13(3). https://doi.org/10.1186/cc7922

14. Ellermann J., Hedderich R., Böcher R., Thauer R. The final step in methane formation. *European Journal of Biochemistry* 1988;172(3):669-677. https://doi.org/10.1111/j.1432-1033.1988.tb13941.x

15. Ernst L., Steinfeld B., Barayeu U., Klintzsch T., Kurth M., Grimm D. et al. Methane formation driven by reactive oxygen species across all living organisms. *Nature* 2022;603(7901):482-487. https://doi.org/10.1038/s41586-022-04511-9

16. Ghyczy M., Torday C., Boros M. Simultaneous generation of methane, carbon dioxide, and carbon monoxide from choline and ascorbic acid - a defensive mechanism against reductive stress?. *The Faseb Journal* 2003;17(9):1124-1126. https://doi.org/10.1096/fj.02-0918fje

17. Hiltebrand L., Krejčí V., tenHoevel M., Banič A., Sigurðsson G. Redistribution of microcirculatory blood flow within the intestinal wall during sepsis and general anesthesia. *Anesthesiology* 2003;98(3):658-669. https://doi.org/10.1097/00000542-200303000-00014

18. Jhanji S., Stirling S., Patel N., Hinds C., Pearse R. The effect of increasing doses of norepinephrine on tissue oxygenation and microvascular flow in patients with septic shock. *Critical Care Medicine* 2009;37(6):1961-1966. https://doi.org/10.1097/ccm.0b013e3181a00a1c

19. Kassavin D., Kuo Y., Ahmed N. Initial systolic blood pressure and ongoing internal bleeding following torso trauma. *Journal of Emergencies, Trauma, and Shock* 2011;4(1):37. https://doi.org/10.4103/0974-2700.76833

20. Kaszaki J., Érces D., Zsikai B., Bizánc L., Nógrády M., Boros,M. Relationship between endogenous methane generation, microcirculatory changes, and superoxide radical production in experimental sepsis. *Shock* 2013;40:36 sppl

21. Keppler F., Hamilton J., Braß M., Röckmann T. Methane emissions from terrestrial plants under aerobic conditions. *Nature* 2006;439(7073):187-191. https://doi.org/10.1038/nature04420

22. Keppler F., Schiller A., Ehehalt R., Greule M., Hartmann J., Polag D. Stable isotope and high precision concentration measurements confirm that all humans produce and exhale methane. *Journal of Breath Research* 2016;10(1):016003. https://doi.org/10.1088/1752-7155/10/1/016003

23. Kim BSM,. Li BT., Engel A., Samra JS,. Clarke S., Norton ID., Li AE. Diagnosis of gastrointestinal bleeding: A practical guide for clinicians. *World Journal of Gastrointestinal Pathophysiology* 2014;5(4):467. https://doi.org/10.4291/wjgp.v5.i4.467

24. Kuebler W., Abels C., Schuerer L., Goetz A. Measurement of neutrophil content in brain and lung tissue by a modified myeloperoxidase assay. *International Journal of Microcirculation* 1996;16(2):89-97. https://doi.org/10.1159/000179155

25. Kumar Y., Hooda K., Li S., Goyal P., Gupta N., Adeb M. Abdominal aortic aneurysm: pictorial review of common appearances and complications. *Annals of Translational Medicine* 2017;5(12):256-256. https://doi.org/10.21037/atm.2017.04.32

26. Kvietys P. The gastrointestinal circulation. Colloquium Series on Integrated Systems Physiology: From Molecule to Function 2010;2(1):1-127. https://doi.org/10.4199/c00009ed1v01y201002isp005

27. Levitt M., Furne J., Kuskowski M., Ruddy J. Stability of human methanogenic flora over 35 years and a review of insights obtained from breath methane measurements. *Clinical Gastroenterology and Hepatology* 2006;4(2):123-129. https://doi.org/10.1016/j.cgh.2005.11.006.

28. Ligor T., Ligor M., Amann A., Ager C., Bachler M., Dzien A. et al. The analysis of healthy volunteers' exhaled breath by the use of solid-phase microextraction and GC-MS. *Journal of Breath Research* 2008;2(4):046006. https://doi.org/10.1088/1752-7155/2/4/046006

29. Liu C. and Zhang J. Methane might be made by all living organisms. *Nature* 2022;603(7901):396-397. https://doi.org/10.1038/d41586-022-00206-3

30. Michaelian KH. Photoacoustic IR spectroscopy: instrumentation, applications and data analysis. New York (NY): John Wiley & Sons; 2010.

31. Ng S., Shi H., Hamidi N., Underwood F., Tang W., Benchimol E.et al. Worldwide incidence and prevalence of inflammatory bowel disease in the 21st century: a systematic review of population-based studies. *The Lancet* 2017;390(10114):2769-2778. https://doi.org/10.1016/s0140-6736(17)32448-0

32. Ngai A., Persijn S., Basum G., & Harren F. Automatically tunable continuous-wave optical parametric oscillator for high-resolution spectroscopy and sensitive trace-gas detection. *Applied Physics* 2006;85(2-3):173-180. https://doi.org/10.1007/s00340-006-2362-3

33. Nose K., Nunome Y., Kondo T., Araki S., Tsuda T. Identification of gas emanated from human skin: methane, ethylene, and ethane. *Analytical Sciences* 2005;21(6):625-628. https://doi.org/10.2116/analsci.21.625

34. Palágyi P., Kaszaki J., Rostás A., Érces D., Németh M., Boros M. et al. Monitoring microcirculatory blood flow with a new sublingual tonometer in a porcine model of hemorrhagic shock. *Biomed Research International* 2015;2015:1-10. https://doi.org/10.1155/2015/847152

35. Pestel G., Fukui K., Kimberger O., Hager H., Kurz A., Hiltebrand L. Hemodynamic parameters change earlier than tissue oxygen tension in hemorrhage. *Journal of Surgical Research* 2010;160(2):288-293. https://doi.org/10.1016/j.jss.2008.11.002

36. Placer Z., Cushman L., Johnson B. Estimation of product of lipid peroxidation (malonyl dialdehyde) in biochemical systems. *Analytical Biochemistry* 1966;16(2):359-364. https://doi.org/10.1016/0003-2697(66)90167-9

37. Qian J., Yang Z., Cahoon J., Xu J., Zhu C., Yang M. et al. Post-resuscitation intestinal microcirculation: its relationship with sublingual microcirculation and the severity of post-resuscitation syndrome. *Resuscitation* 2014;85(6):833-839. https://doi.org/10.1016/j.resuscitation.2014.02.019

38. Rutgeerts P., Assche G., Vermeire S. Optimizing anti-TNF treatment in inflammatory bowel disease. *Gastroenterology* 2004;126(6):1593-1610. https://doi.org/10.1053/j.gastro.2004.02.070

39. Steigleder K., Neto F., Nagasako C., Leal R. Anti-integrins, anti-interleukin 12/23p40, and JAK inhibitors for the inflammatory bowel disease treatment. *Biological Therapy for Inflammatory Bowel Disease.* IntechOpen; 2020. https://doi.org/10.5772/intechopen.90536

40. Szűcs S., Bari G., Ugocsai M., Lashkarivand R., Lajkó N., Mohácsi Á. et al. Detection of intestinal tissue perfusion by real-time breath methane analysis in rat and pig models of mesenteric circulatory distress. *Critical Care Medicine* 2019;47(5):e403-e411. https://doi.org/10.1097/ccm.0000000000003659

41. Tasu J., Vesselle G., Herpe G., Ferrié J., Chan P., Boucebci S. et al. Postoperative abdominal bleeding. *Diagnostic and Interventional Imaging* 2015;96(7-8):823-831. https://doi.org/10.1016/j.diii.2015.03.013

42. Tuboly E., Szabó A., Erős G., Mohácsi Á., Szabó G., Tengölics R. et al. Determination of endogenous methane formation by photoacoustic spectroscopy. *Journal of Breath Research* 2013;7(4):046004. https://doi.org/10.1088/1752-7155/7/4/046004

43. Ugocsai M., Bársony A., Varga R., Gajda Á., Vida N., Lajkó N. et al. Conjugation with tris decreases the risk of ketoprofen-induced mucosal damage and reduces inflammation-associated methane production in a rat model of colitis. *Pharmaceutics* 2023;15(9):2329. https://doi.org/10.3390/pharmaceutics15092329

44. Wang Q., Alowaifeer A., Kerner P., Balasubramanian N., Patterson A., Christian W. et al. Aerobic bacterial methane synthesis. *Proceedings of the National Academy of Sciences* 2021;118(27). https://doi.org/10.1073/pnas.2019229118

45. Wu C., Chan K., Cheng Y., Yeh Y., Chien C. Effects of different types of fluid resuscitation for hemorrhagic shock on splanchnic organ microcirculation and renal reactive oxygen species formation. *Critical Care* 2015;19(1). https://doi.org/10.1186/s13054-015-1135-y

46. Yu Y. and Pawliszyn J. On-line monitoring of breath by membrane extraction with sorbent interface coupled with CO_2 sensor. *Journal of Chromatography* 2004;1056(1-2):35-41. https://doi.org/10.1016/s0021-9673(04)01828-x

8 ACKNOWLEDGEMENT

I would like to express my sincere gratitude to Andrea Szabó, Head of the Institute of Surgical Research, for the invaluable opportunity to work in his department and for his scientific guidance throughout this project.

Special thanks to Professor Mihály Boros, the formal Head of the Institute of Surgical Research, for his continuous support and guidance during my scientific work and supervising my papers.

I am grateful to Gabriella Varga and Dániel Érces for the basic research idea and their invaluable contribution to my experimental work and their guidance throughout the preparation of my thesis.

I am grateful to the staff at the Institute of Surgical Research for their outstanding technical assistance and to all my colleagues for their collaboration and support.

I sincerely thank Professor Gábor Tóth, Head of the Department of Medical Chemistry, University of Szeged for the conjugation of the newly developed NSAID derivatives.

This research was funded by the grants EFOP-3.6.2-16-2017-00006 (MB) and 2024-1.2.3-HU-RIZONT-2024-00033 which has been implemented with the support provided by the Ministry of Culture and Innovation of Hungary from the National Research, Development and Innovation Fund, financed under the 2024-1.2.3-HU-RIZONT funding scheme.

Finally, I wish to thank my Family and my Parents for their boundless love, patience, and trust, which have been my greatest sources of strength throughout this journey.

ANNEX I.

ANNEX II.